THE GEOLOGICAL SOCIETY OF AMERICA®

Patterns of incision and deformation on the southern flank of the Yellowstone hotspot from terraces and topography

Daphnee Tuzlak[1], Joel Pederson[1,†], Aaron Bufe[2], and Tammy Rittenour[1]
[1]*Department of Geosciences, Utah State University, 4505 Old Main Hill, Logan, Utah, 84322, USA*
[2]*GFZ German Research Centre for Geosciences, Telegrafenberg, 14473 Potsdam, Germany*

ABSTRACT

Understanding the dynamics of the greater Yellowstone region requires constraints on deformation spanning million year to decadal timescales, but intermediate-scale (Quaternary) records of erosion and deformation are lacking. The Upper Snake River drainage crosses from the uplifting region that encompasses the Yellowstone Plateau into the subsiding Snake River Plain and provides an opportunity to investigate a transect across the trailing margin of the hotspot. Here, we present a new chronostratigraphy of fluvial terraces along the lower Hoback and Upper Snake Rivers and measure drainage characteristics through Alpine Canyon interpreted in the context of bedrock erodibility. We attempt to evaluate whether incision is driven by uplift of the Yellowstone system, subsidence of the Snake River Plain, or individual faults along the river's path. The Upper Snake River in our study area is incising at roughly 0.3 m/k.y. (300 m/m.y.), which is similar to estimates from drainages at the leading eastern margin of the Yellowstone system. The pattern of terrace incision, however, is not consistent with widely hypothesized headwater uplift from the hotspot but instead is consistent with downstream baselevel fall as well as localized deformation along normal faults. Both the Astoria and Hoback faults are documented as active in the late Quaternary, and an offset terrace indicates a slip rate of 0.25–0.5 m/k.y. (250–500 m/m.y.) for the Hoback fault. Although tributary channel steepness corresponds with bedrock strength, patterns of χ across divides support baselevel fall to the west. Subsidence of the Snake River Plain may be a source of this baselevel fall, but we suggest that the closer Grand Valley fault system could be more active than previously thought.

†Corresponding author: joel.pederson@usu.edu.

INTRODUCTION

The greater Yellowstone region is one of the most rapidly deforming areas in the North American continent and encompasses one of Earth's most famous volcanic systems (e.g., Smith and Braile, 1994; Pierce and Morgan, 2009; Smith et al., 2009). Understanding the evolution and dynamics of this complex system requires a combination of studies across decadal to million year timescales. Diverse data sets have documented the northeast migration of the magmatic center over the late Cenozoic and the formation of the Snake River Plain by subsidence and crustal extension in the wake of the uplift (e.g., Anders and Sleep, 1992; McQuarrie and Rodgers, 1998; Rodgers et al., 2002; Anders et al., 2014) (Fig. 1). At the other end of the timescale, the present-day pattern of thermal-magmatic and dynamic uplift around the Yellowstone Plateau has been extensively studied using geodetic techniques and models (e.g., Chang et al., 2007; Smith et al., 2009; Pierce and Morgan, 2009; Becker et al., 2014; Huang et al., 2015; Tizzani et al., 2015). However, intermediate, Quaternary timescale data on the uplift and erosion of the greater Yellowstone region exist only for the leading margin of the hotspot and are limited in their quantitative constraints (Reheis, 1985; Dethier, 2001; Pierce and Morgan, 2009; Guerrero, 2016). This knowledge gap of the intermediate timescale needs to be filled before geodynamic models for the evolution of the Yellowstone system can be tested.

Here we present a geomorphic analysis and a chronostratigraphy of fluvial terraces along the Hoback River and the Snake River below their confluence, which forms an E-W transect south of Jackson Hole to Alpine, Wyoming, USA (Fig. 1). This transect crosses from the hypothetically uplifting terrain around the leading edge of the hotspot to the subsiding Snake River Plain and presents an opportunity to document rates of Quaternary deformation across the region. We combine measurements of the age and geometry of three levels of fluvial terraces with long profile analysis of the Upper Snake River and local tributaries. After accounting for the effect of varying rock strength on river profiles and climate cycles on terrace development, we aim to decipher to what degree the Quaternary evolution of the Snake River is driven by (1) broad, transient uplift around the Yellowstone hotspot; (2) subsidence of the Snake River Plain; or (3) deformation along individual normal faults.

BACKGROUND AND APPROACH

Yellowstone Geodynamics

The area of the greater Yellowstone region is thought to be dynamically uplifting due to the rising plume of the Yellowstone hotspot (Lowry et al., 2000; Pierce and Morgan, 2009; Becker et al., 2014). This is one of the most seismically active areas of the western U.S., and it is characterized by a relatively thin and low-density crust with sub-crustal heat flow of ~30 times the global continental average (Smith and Braile, 1994). The Yellowstone Caldera, the site of the most recent volcanism in the region, continues to actively deform with vertical surface motions of 1–2 cm/yr between 1923 and 2004 and as high as 7 cm/yr between 2004 and 2006 (Chang et al., 2007, 2010; Tizzani et al., 2015).

Over the past 17 m.y., the North American Plate has moved southwest with respect to the hotspot and created a northeastward-extending track that is characterized by extensive magmatism and faulting (e.g., Pierce and Morgan, 2009; Anders et al., 2014). A northeastward progression in exhumation has been interpreted via thermochronological data following this progression of magmatism and uplift from the hotspot (Vogl et al., 2014). In the wake of this plume, the Snake River Plain has been subsiding due to subsequent emplacement of a thick, dense, mafic succession in the middle crust as well as cooling and thermal contraction (Anders and Sleep, 1992; McQuarrie and Rodgers, 1998; Rodgers et al., 2002). Topographic relief between the Yellowstone Plateau and the eastern Snake River Plain is ~1300 m

GSA Bulletin; May/June 2022; v. 134; no. 5/6; p. 1319–1333; https://doi.org/10.1130/B35923.1; 10 figures; 1 table; 1 supplemental file.
published online 9 September 2021

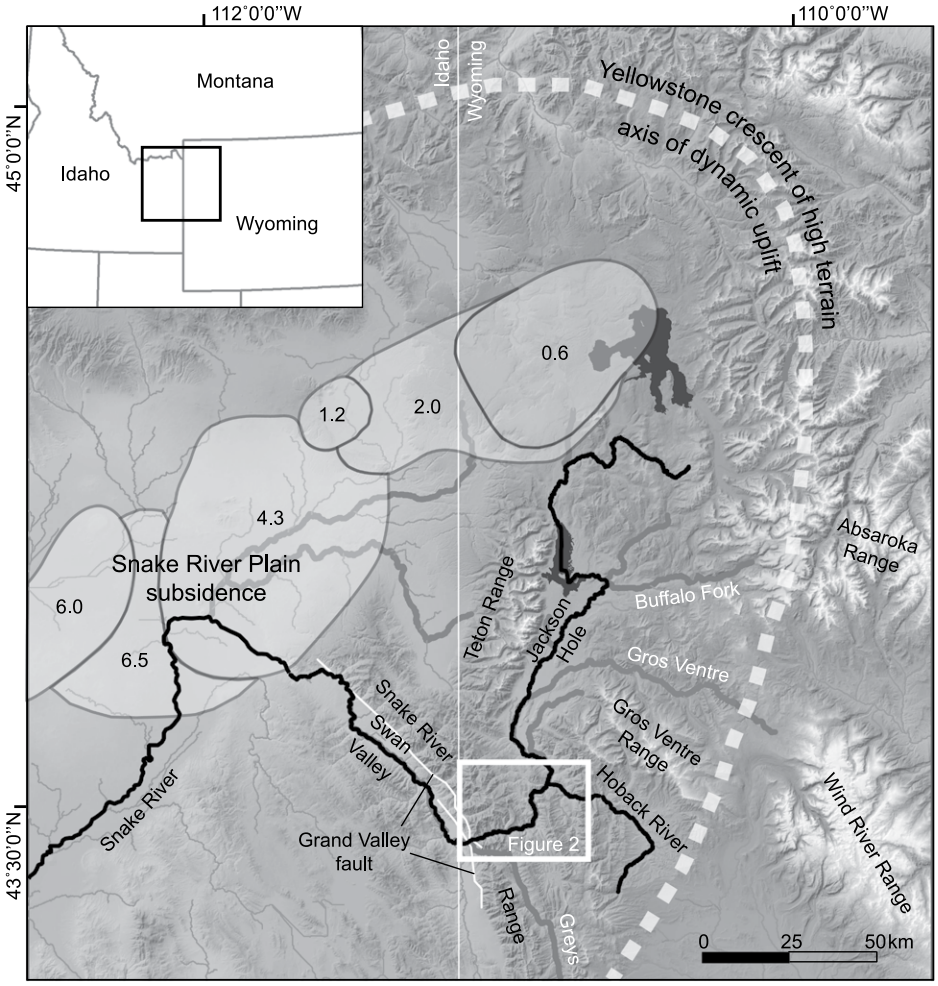

Figure 1. Location map shows the Upper Snake River and Yellowstone region. Grey encircled areas are volcanic fields of the Snake River Plain, and ages (in Ma) denote their times of activity; included are the Heise volcanic field (6.5–4.3 Ma) and Yellowstone Plateau volcanic field (2.0–0.6 Ma) (modified from Smith and Braile, 1994, and Link et al., 2005). The axis of the hypothetical Yellowstone crescent of high terrain (white dashed line) traces an arch of potential dynamic uplift around the leading margin of the Yellowstone hotspot (modified from Pierce and Morgan, 2009). Gray lines highlight major tributaries of the Snake River and Hoback River (black lines). White box outlines study area depicted in Figure 2.

(Fig. 1) (Smith and Braile, 1994), and total subsidence of the Snake River Plain relative to the adjacent northeastern Basin and Range Province is 4.5–8.5 km according to flexural profiles (McQuarrie and Rodgers, 1998). Subsidence of the Snake River Plain is reflected in drainage capture into the Snake River Plain and the migration of divides during the middle to late Pleistocene (Rodgers et al., 2002; Wegmann et al., 2007). Detrital zircon provenance studies suggest that the Upper Snake River joined the Snake River Plain basin only within the last 2.5 m.y. (Link et al., 2005; Beranek et al., 2006).

In overview, studies have constrained the Cenozoic history of the Yellowstone region from the Laramide orogeny (Peyton et al., 2012; Stevens et al., 2016) to the Neogene (McQuarrie and Rodgers, 1998; Vogl et al., 2014) as well as the modern deformation patterns (Chang et al., 2007, 2010; Tizzani et al., 2015). In contrast, inferences about late Quaternary uplift and erosion remain limited to the northern and eastern margins of the hotspot (Reheis, 1985; Dethier, 2001; Sharp et al., 2003; Pierce and Morgan, 2009; Guerrero, 2016). Longer-term incision rates since the 640 ka Lava Creek B tephra eruption are broadly >150 m/m.y. (Reheis, 1985; Dethier, 2001), and Sharp et al. (2003) calculated incision rates of 180 ± 60 m/m.y. from terraces along the Wind River off to the southeast of Yellowstone. Stream terraces converging downstream from the Absaroka Range into the Bighorn and Wind River Basins to the east have been interpreted as evidence for differential, transient uplift of the inferred Yellowstone crescent of high terrain with roughly estimated uplift rates of 100 m/m.y. along the crest of this arch of high topography (Pierce and Morgan, 2009; Guerrero, 2016). Other broad estimates of uplift on the eastern side of the Yellowstone Plateau range from 100 m/m.y. to 400 m/m.y. based on the incision of volcanic rocks and late Pleistocene changes in reconstructed equilibrium line altitudes (Pierce and Morgan, 2009). Although the leading margin of the Yellowstone system seems to exhibit this pattern of broad, transient uplift and differential Quaternary river incision, the trailing, southwestern margin instead may be influenced by the subsidence of the Snake River Plain. In addition, a number of individual mountain ranges with range-bounding and other, active normal faults may lead to shorter-wavelength, more localized patterns of deformation (Fig. 1).

Fluvial Terraces and Longitudinal Profiles as Tectonic Markers

To reconstruct Quaternary deformation on the trailing margin of the Yellowstone hotspot, we first analyze the geometry and age of fluvial terraces along the Snake and Hoback Rivers. Fluvial terraces are abandoned channel beds and deposits that form when incising rivers experience a variation in sediment discharge or hydrologic conditions. In pro-glacial settings such as our study area, large variations in water and sediment discharges during climate changes commonly cause cycles of lateral planation and strath cutting, aggradation, and incision (Hancock and Anderson, 2002; Bridgland and Westaway, 2008; Gibbard and Lewin, 2009; Malatesta et al., 2018). Even though the timing of terrace formation is sensitive to the beat of climate changes, a stratigraphy of terraces provides valuable tectonic markers that can record the average rate and pattern of deformation (Merritts et al., 1994; Burbank et al., 1996; Pazzaglia et al., 1998; Gallen et al., 2015). For example, terraces that form during uplift in the headwaters of a river tend to converge downstream such as those interpreted by previous workers along the leading margin of Yellowstone. Conversely, differential downstream baselevel fall triggers upstream-migrating incision, which forms terraces that diverge downstream (Merritts et al., 1994; Kirby and Whipple, 2001; Wegmann and Pazzaglia, 2009; Gran et al., 2013).

In addition to fluvial terraces, we use the width, steepness, and stream power of the Upper Snake River and the steepness of its tributaries to explore incision patterns. Bedrock chan-

nels adjust their slope and width to generate the stream power sufficient to incise at the rate of long-term baselevel fall (e.g., Wobus et al., 2006; Kirby and Ouimet, 2011; Kirby and Whipple, 2012), and unit stream power is the rate of potential energy loss of the flow against its bed:

$$\Omega_u = \frac{\rho g Q S}{w}, \quad (1)$$

where ρ is the density of water, g is gravity, Q is discharge, S is the slope, and w is the channel width (Howard and Kerby, 1983). Steepness indexes for analyzing reach-scale channel profiles are, in turn, based on the stream-power erosion model that is derived from Equation 1. This model includes the normalized steepness index (k_{sn}), which is quantified using a power-law relationship between channel gradient (S) and upstream drainage area (A) with a reference concavity (θ_n) (Flint, 1974; Kirby and Whipple, 2012):

$$S = k_{sn} A^{-\theta_n}. \quad (2)$$

Studies demonstrate that bedrock channels narrow and steepen with increasing uplift rates and that channel steepness and width are also influenced by sediment supply, discharge, and bedrock lithology (Burbank et al., 1996; Finnegan et al., 2007; Yanites and Tucker, 2010; Whipple et al., 2013). In particular, variations in rock strength can obscure or mimic tectonic signatures. Narrower, steeper channels occur in more resistant bedrock (Montgomery and Gran, 2001; Whipple, 2004; Bursztyn et al., 2015), and experimental and field studies show that erosion rates vary inversely with the square of the tensile strength (Sklar and Dietrich, 2001). In this study, we analyze channel steepness and morphology in the context of changes in underlying bedrock strength in an attempt to isolate the tectonic effect on channel profile geometry.

We also use the distribution of knickpoints or knickzones that are separating channel reaches with different steepness. These knickpoints can be anchored in space and separate reaches with different lithology or uplift rate (Miller, 1991; Goldrick and Bishop, 1995; Duvall et al., 2004; Kirby and Whipple, 2012), or they can reflect transient incision of the channel profile to a downstream change in baselevel (Whipple et al., 2013). Importantly, knickpoints in different tributaries that were generated from the same downstream disturbance are typically found at a similar elevation (Crosby and Whipple, 2006; Gallen et al., 2013). Hence, we use the distribution of knickpoints in comparison with elevation and lithologic boundaries to unravel tectonic and lithologic controls on channel profiles.

The final metric that we use to analyze the stream network is χ (Chi), an inverse integral of the drainage area (Perron and Royden, 2013):

$$\chi = \int_{x_b}^{x} \left(\frac{A_0}{A(x)} \right)^{-\theta_n} \mathrm{dx}, \quad (3)$$

where A_0 is a reference drainage area. Equilibrium stream profiles that are adjusted to the same boundary conditions are co-linear in chi-elevation space, and knickpoints can be identified as breaks in slope in chi-elevation space. Also, comparisons of χ values across drainage divides are commonly used as a metric for the stability of these divides (Willett et al., 2014). Stable divides are characterized by values that are similar across the divide. A mismatch in χ divides tends to indicate a migration of the divide from lower to higher χ values unless a contrast in lithology or uplift rates across the divide maintains the disequilibrium in χ values (Willett et al., 2014).

Study Area

The headwaters of the Snake River are in the Absaroka Range and the Yellowstone Plateau of northwestern Wyoming (Fig. 1). Downstream, the Snake River flows parallel to the Teton Range through Jackson Hole and flows south into a low-relief canyon to its confluence with the Hoback River, which is the major westward-flowing tributary. Approximately 5.5 km downstream of Hoback Junction, the Snake River turns south along a wide alluvial reach before again turning west against the bedrock structural grain and cutting the 1-km-deep Alpine Canyon through the Snake River Range (Fig. 1). Finally, the Snake crosses the Alpine segment of the Grand Valley fault and flows north through Swan Valley before draining into the eastern Snake River Plain. The Hoback River forms the upstream portion of our E-W study transect and drains part of the Wyoming and Gros Ventre Ranges along the hypothetical Yellowstone crescent of high terrain. Upstream of the Hoback normal fault, the river runs in a narrow bedrock canyon through Paleozoic carbonates, whereas downstream it crosses a small Neogene basin through a wider valley into the Snake River (Fig. 2).

Our study focuses on the Snake River between Hoback Junction and Alpine, Wyoming, where the most extensive terraces are preserved. Previous studies proposed that the terraces in Alpine Canyon could be traced to glacial deposits in Jackson Hole (Walker, 1964; Stoll, 1991). Reconstructions of past glaciations show that the marine isotope stage (MIS) 6 (Bull Lake) ice sheet from the Yellowstone Plateau extended across Jackson Hole to a morainal ridge just 2 km north of Hoback Junction, where cosmogenic-exposure ages have been recently recalculated to 150 ± 4 ka (Licciardi and Pierce, 2018). The MIS 2 (Pinedale) glaciation was less extensive, and Pinedale moraines of the southern Yellowstone glacial system range in age from 16 ka to 14 ka, and the outermost moraines are in Jackson Hole ~35–55 km upstream of the study area (Licciardi and Pierce, 2018; Pierce et al., 2018). Given this proglacial setting, we expect the formation of terraces along Alpine Canyon to be linked to glacial cycles (Hancock and Anderson, 2002).

Geologically, the Snake River Range surrounding Alpine Canyon lies in a thrust belt that developed during the Sevier Orogeny in middle Cretaceous time (Heller et al., 1986). Lower Paleozoic carbonates on the west side of the range are sequentially thrust over upper Paleozoic and then more siliciclastic Mesozoic sedimentary rocks to the east (Fig. 2). This thick and diverse sedimentary section has subsequently undergone extensional faulting especially along the range-bounding Grand Valley fault to the west. The Grand Valley fault was most active at 5–2 Ma, and documented evidence for significant Quaternary slip is limited to the Star Valley south of Alpine Canyon (Anders et al., 1989; Piety et al., 1992; Pierce and Morgan, 2009) (Fig. 1). In addition, a few previously recognized but poorly studied faults lie upstream of Alpine Canyon along the fluvial transect of this study. The south-striking Astoria normal fault system downstream of Hoback Junction cuts across Pleistocene gravels and was potentially active before and after Quaternary gravel deposition (Fig. 2 and Item S1[1]) (D. Rodgers and S. Wood, 2016, personal commun.). The similarly oriented Hoback normal fault east of Hoback Junction was active in several episodes between the late Miocene and Pliocene (Dorr et al., 1977, 1987) and created a basin that was filled with Neogene conglomerates. Quaternary activity of this southern segment of the fault has not been previously documented.

Sources of Baselevel Fall Along the Snake River

We recognize three possible sources of baselevel changes that may affect the Upper Snake and Hoback Rivers: (1) broad uplift of the

[1]Supplemental Material. Item 1: Surficial map of Alpine Canyon, Item 2: OSL data, Item 3: Bedrock Strength. Please visit https://doi.org/10.1130/GSAB.S.15101424 to access the supplemental material, and contact editing@geosociety.org with any questions.

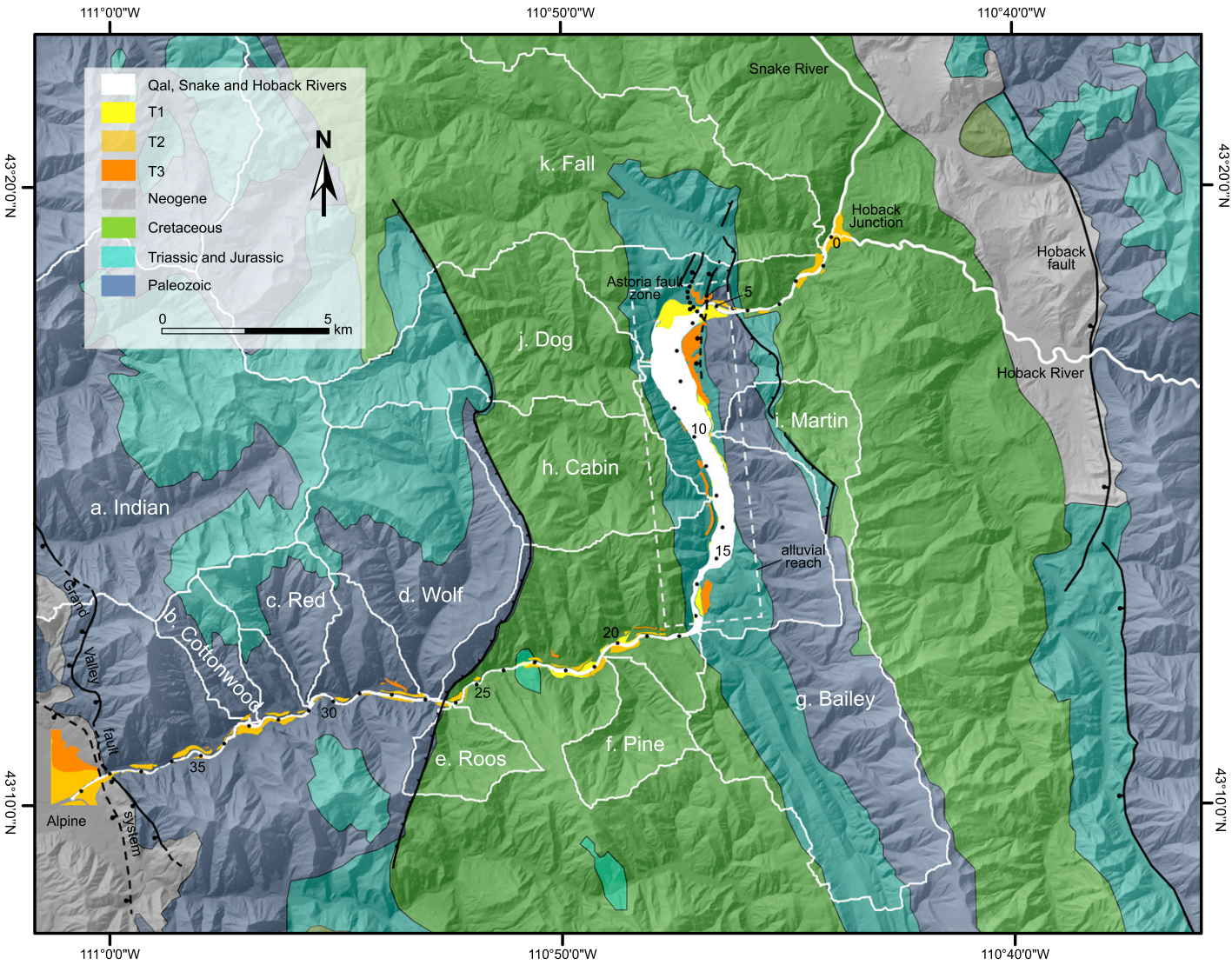

Figure 2. Study area includes Alpine Canyon of the Snake River upstream to Hoback Junction and the lower Hoback River. Faults and underlying geologic units generalized by age are taken from the 1:500,000 scale Wyoming state map (USGS, 2005). Black dots along the river denote river km through Alpine Canyon, where the confluence with the Hoback River is 0. Note the distinct upper bedrock reach (river km 0–5.5), dashed box marking the wide central alluvial reach (river km 5.5–17), and the lower bedrock reach (river km 17–39). Selected tributary catchments are outlined in light gray: (a) Indian Creek, (b) Cottonwood Creek, (c) Red Creek, (d) Wolf Creek, (e) Roos Creek, (f) Pine Creek, (g) Bailey Creek, (h) Cabin Creek, (i) Martin Creek, (j) Dog Creek, and (k) Fall Creek.

headwater region, and (2) subsidence of the eastern Snake River Plain, are expected to act on wavelengths of several tens to hundreds of kilometers whereas (3) slip on the Grand Valley, Astoria, and Hoback normal faults could affect river incision patterns at shorter wavelengths. These three sources of deformation are expected to lead to distinct, hypothetical long profile and terrace patterns (Fig. 3, inset). Uplift of the headwaters along the Hoback River and Yellowstone crescent of high terrain should lead to broadly tilted terraces that converge downstream (inset a). With subsidence of the eastern Snake River Plain, we would expect an upstream-migrating, baselevel fall signal with an upstream decrease of incision and, potentially, the preservation of a relict or buffered upper drainage reach along the mainstem that has not yet experienced the baselevel signal (Fig. 3, inset b). Finally, local baselevel fall signals from activity on normal faults should be recorded by offset of terrace markers on length scales of a few kilometers with reduced incision in the hanging wall near faults (Fig. 3, inset c). Active faults could also generate knickpoints upstream of the faults that are clustered at similar elevations across the tributary network (Crosby and Whipple, 2006; Gallen et al., 2013). In a complex reality, we may expect more than one source of baselevel fall that results in a combination of these end-member patterns expressed at different wavelengths in the landscape.

METHODS

In the focus area between Hoback Junction and the town of Alpine, surficial deposits were mapped at a 1:12,000 scale along the corridor of the canyon bottom to document all fluvial-terrace deposits and their stratigraphic relations with tributary debris fans, landslides, and colluvium (Item S1). The heights of fluvial terrace

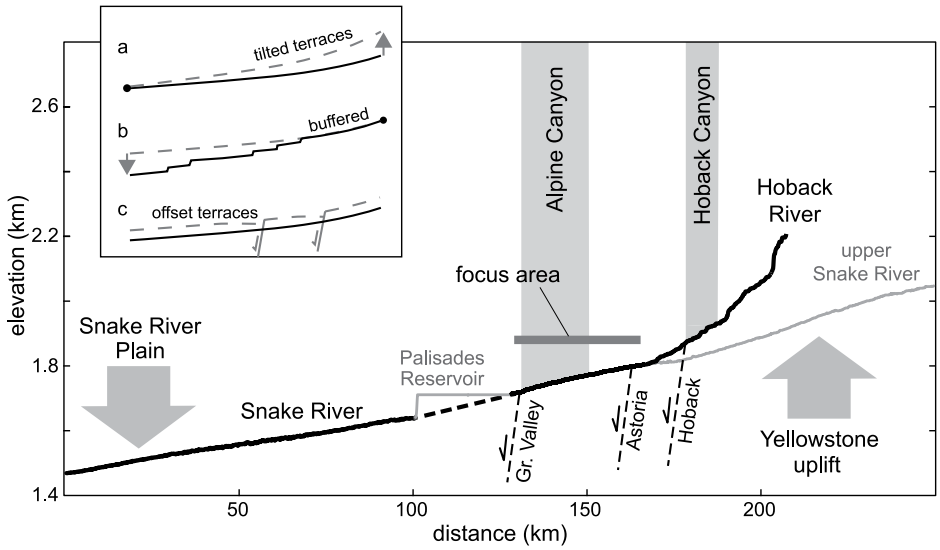

Figure 3. Longitudinal profile is from 10 m U.S. Geological Survey national elevation data set digital elevation model of the Snake River and its Hoback River tributary from headwaters draining off the potentially uplifting Yellowstone crescent of high terrain, through the faulted study reaches including Hoback Canyon and the focused study area through Alpine Canyon, to an arbitrary point in the subsiding Snake River Plain. Inset illustrates conceptual model distinguishing sources of baselevel fall and attendant patterns of incision: (a) river terraces tilt and converge downstream due to long wavelength uplift in headwaters; (b) terraces diverge downstream due to propagation of incision from subsidence; and (c) terraces are offset at short wavelengths by local normal faulting.

deposits were surveyed relative to the river surface at a discharge of 95 m^3/s (3350 ft^3/s), and terrace deposits were correlated by their landscape position as well as by geochronology. Major units mapped as $Qag_{1–3}$ represent three generations of fluvial terrace deposits, and units $Qagp_{1–3}$ comprise piedmont/tributary fan deposits graded to the terraces and various hillslope deposits (Tuzlak, 2017; Item S1). Both strath and fill terraces were distinguished in the study area. Strath terraces are planar bedrock surfaces with a typically thin (<10 m) alluvial cover, whereas fill terraces have an alluvial cover thicker than the system's typical channel depth and often a less planar bedrock strath. River terrace deposits are designated T1 (youngest), T2, and T3 (oldest), and piedmont/tributary fan deposits are referred to as P1 (youngest), P2, and P3 (oldest) for mapping purposes. Upstream of the focus area along the Hoback River, fluvial terraces were mapped and surveyed on Google Earth and in the field and correlated by geochronology and strath height to Snake River terraces.

Age control for river terraces was obtained using optically stimulated luminescence (OSL) dating of quartz sand (Huntley et al., 1985). OSL provides an age estimate of the time since a sediment grain was last exposed to sunlight (Rhodes, 2011) and therefore represents depositional ages. Samples were collected by pounding metal tubes into sand lenses. Sample USU-2296 was collected in a lightproof container at night under red light due to the lack of sand lenses at this site (Table 1). Sample sites were chosen >1 m below the geomorphic surface and among primary sedimentary structures to avoid bioturbation. Samples were analyzed at the Utah State University Luminescence Lab using the single aliquot regenerative-dose (SAR) protocol (Murray and Wintle, 2000), and ages were calculated with a central age model (Table 1; for detailed methods and results see Item S2; see footnote 1). Proglacial fluvial settings, such as were sampled here, are not ideal conditions for solar resetting (bleaching) of the luminescence signal (Fuchs and Owen, 2008). However, the effect of residual signals in samples >15 ka may be negligible in comparison to the dose obtained during burial (Jain et al., 2004; Fuchs and Owen, 2008; Rittenour, 2008). Nevertheless, we used small aliquot analysis and monitored for skewness and high overdispersion in the data to test for effects of partial bleaching (incomplete solar resetting) and age overestimation.

The suite of Paleozoic and Mesozoic sedimentary rocks in the focus area between Hoback Junction and the town of Alpine was

TABLE 1. HOBACK RIVER AND ALPINE CANYON TERRACE OPTICALLY STIMULATED LUMINESCENCE (OSL) GEOCHRONOLOGY

Deposit*	Location	Sample #	Latitude (°N)	Longitude† (°W)	Depth (m)§	# Aliquots (total)#	Dose rate ($Gyky^{-1}$)	Equivalent dose ± 2σ (Gy)**	OSL age ± 1σ (ka)
P1	Above Cabin Creek	USU-2106	43°14'59"	110°46'39"	2	15 (17)	3.65 ± 0.20	5.35 ± 1.55	1.46 ± 0.26
T2	Boy Scout Camp	USU-2079	43°18'36"	110°44'40"	3.5	20 (42)	2.40 ± 0.13	27.83 ± 1.79	11.60 ± 1.21
T2	West Table Camp	USU-2020	43°12'34"	110°48'32"	1.3	22 (34)	2.26 ± 0.12	28.24 ± 3.64	12.49 ± 1.47
T2	Below Cabin Creek	USU-2302	43°14'50"	110°46'36"	10	18 (22)	2.11 ± 0.12	29.08 ± 3.16	13.79 ± 1.58
T2	Downstream Hoback fault	USU-2296††	43°17'11"	110°39'6"	0.8	12 (33)	1.67 ± 0.07	23.42 ± 2.77	14.01 ± 1.40
T2	Mouth of Hoback River	USU-2294	43°19'7"	110°43'27"	0.9	16 (33)	2.37 ± 0.10	36.03 ± 3.26	15.19 ± 1.41
T2	Hoback Canyon	USU-2295	43°17'10"	110°32'21"	3.2	17 (34)	2.23 ± 0.11	41.99 ± 4.58	18.82 ± 1.92
T2	Near Alpine	USU-1999	43°10'32"	110°59'53"	20	19 (42)	2.12 ± 0.13	48.35 ± 3.96	22.78 ± 2.48
T2	Upstream Hoback fault	USU-2293	43°17'16"	110°37'60"	2.5	16 (23)	1.58 ± 0.06	40.42 ± 3.84	25.58 ± 2.40
T3	Astoria (lower)	USU-2080	43°18'11"	110°46'46"	40	22 (33)	2.22 ± 0.12	152.8 ± 21.31	68.97 ± 8.49
T3	Near Alpine	USU-2019	43°10'52"	111°01'12"	15	20 (28)	2.84 ± 0.16	202.82 ± 28.93	71.37 ± 8.85
T3	Astoria (upper)	USU-2303	43°18'12"	110°46'45"	25	15 (35)	1.81 ± 0.10	146.51 ± 35.83	77.56 ± 11.33
T3	Sporting Club Gravel Pit	USU-1996	43°16'32"	110°46'48"	4.7	22 (41)	2.64 ± 0.15	245.55 ± 39.22	92.86 ± 11.94
T3	Sporting Club Roadcut	USU-1998	43°17'30"	110°47'17"	>20	19 (35)	1.54 ± 0.08	149.94 ± 24.18	97.21 ± 12.54

*Organized by stratigraphic position along the Hoback River and Snake River.
†NAD83.
§Depth refers to the stratigraphic distance below the upper surface.
#Age analysis using the single-aliquot regenerative dose procedure of Murray and Wintle (2000) on 1 mm small aliquots of quartz sand. Number of aliquots used in age calculation and number of aliquots analyzed are in parentheses.
**Equivalent dose (D_E) calculated using the Central Age Model (CAM) of Galbraith and Roberts (2012).
††Due to the absence of sand lenses, sand was collected at night under a red light.

generalized from prior mapping (Stoeser et al., 2005) into five bedrock groups for analysis of bedrock strength: Group 1 comprises lower Paleozoic carbonates (Gros Ventre, Gallatin, and Bighorn Formations), Group 2 includes middle-upper Paleozoic carbonates (Darby, Lodgepole, Mission Canyon, Wells, and Phosphoria Formations), Group 3 are lower Mesozoic mixed-lithology sedimentary rocks (Dinwoody, Woodside, Ankareh, Thaynes, Nugget, and Gypsum Spring Formations), Group 4 comprises middle Mesozoic sedimentary rocks (Twin Creek, Pruess, and Stump Formations), and Group 5 includes upper Mesozoic sandstone and shale (Gannet Group and the Bear River and Aspen Formations). Bedrock strength was estimated using the Selby rock mass strength (RMS) classification and included Schmidt hammer measurements and fracture/bedding spacing (Selby, 1993; Tuzlak, 2017). In addition, the percentage of shale, sandstone/siltstone, and limestone of each formation was tallied from the measured stratigraphic sections of Wanless (1955) in the Snake River Range.

Topographic surveys in the focus area included measuring the longitudinal water surface profile of the Snake River with a survey-grade GPS fixed to a raft. In the lower few kilometers of Alpine Canyon, where the river enters Palisades Reservoir, the river profile was reconstructed from historic data as described in Tuzlak (2017). The profile of the Hoback River was extracted and compiled from 1:24,000 scale U.S. Geological Survey topographic maps (U.S. Geological Survey, 1965) and a 10 m USGS national elevation data set (NED) digital elevation model (DEM), and terrace heights were measured with a laser rangefinder and clinometer.

A 500 m, reach-averaged width along the Snake River was calculated by dividing the area of the active channel from orthophoto imagery by the length of the channel centerline. Unit stream power was likewise averaged for 500 m reaches of the Snake River based on the reconstructed 2 yr recurrence peak discharge, the channel width, and the channel slope from the river survey. The 2 yr peak flow was obtained from streamflow data in Alpine Canyon (USGS gage number 13022500) and adjusted to account for the influence of the Jackson Lake Dam upstream. Detailed hydrologic methods are found in Tuzlak (2017).

Channel steepness and chi analysis of long profiles of the channel were conducted across the focused study area around Alpine Canyon with a 10 m USGS NED DEM processed in ArcGIS and TopoToolbox2 in MATLAB (Schwanghart and Scherler, 2014). We used drainages with contributing areas >1 km^2, a segment length of 1000 m, and a reference concavity (θ_n) of 0.45.

RESULTS

Mapping and Correlation of Terraces

The Hoback and Upper Snake Rivers can be partitioned into distinct bedrock reaches that are defined by exposed bedrock on the channel bed and banks and separated by alluvial reaches characterized by banks and beds of alluvium. Upstream to downstream along the Hoback River, we distinguish between a steep bedrock canyon upstream of the Hoback fault, the Neogene alluvial basin in the hanging wall of the Hoback fault, and the lower Hoback valley entrenched into bedrock. Along the Snake River in the study area, we distinguish between an upper bedrock canyon that continues from the Hoback River confluence down to Snake River km 5.5 (where km 0 is the confluence), a wider braided alluvial reach spanning Snake River km 5.5–17, and the Alpine bedrock canyon between Snake River km 17–39 and ending at Palisades Reservoir (Fig. 2). Mapping of the channel and its surficial deposits reveals that preservation and form of fluvial terraces are distinctly different between the bedrock and alluvial reaches (Fig. 2 and Item S1). Bedrock reaches have narrow, single-thread channels, a relatively small valley width, and prominently preserved T2 strath terraces that are frequently buried beneath tributary and slope deposits (Figs. 4–5). In contrast, the alluvial reaches are characterized by channels that are set within a wider valley and can become braided. The alluvial reaches coincide with the thickest fill-terrace deposits.

Two primary Pleistocene terrace deposits, T3 and T2, are recognized in the study area based on the height above the modern channel and on geochronology. A relatively thin, younger T1 gravel was also identified and is most common in the alluvial reach (Fig. 2; Item S1). Terrace deposits are clast-supported, with rounded, imbricated pebbles and cobbles and a few lenticular, moderately sorted, cross-bedded sand lenses. Some terraces are covered by loess that can be >10 m thick as is the case for the T3 terrace near Alpine.

The T3 deposit is most prominent in the alluvial reaches and at Alpine, but remnants can be found through Alpine Canyon (Fig. 2). Along the lower Hoback River, no major remnants of T3 were identified. At the occurrence of T3 furthest upstream, on the river right bank at Astoria (river km 5.5), the deposit is 84 m thick. The preserved T3 deposit thins downstream to $\sim$35 m along the alluvial reach and to $\sim$30 m at the mouth of the canyon near Alpine (Fig. 4). In contrast to T3, the T2 gravel is well preserved in all bedrock reaches from the lower Hoback River to the mouth of Alpine Canyon. The T2 terraces are covered by $\sim$5–16 m of fill. A lower bench cut into T2 deposits (fill-cut terrace T2y) is recognized in several places and can explain the thickness variation of the fill (Fig. 4; Item S1). The lowest and youngest T1 terrace deposit is situated above the modern channel and has a fill thickness of 2–6 m and is best preserved in the alluvial reach. At the downstream end of the lower bedrock canyon, such as at Snake River km 34, the T1 terrace is exposed as a beveled bedrock strath $\sim$6 m above the height of the modern water surface.

The height of the basal strath of fluvial terraces above the modern channel changes along the river course and is best illustrated by the T2, which has the most continuous exposure and varies between 4 m and 13 m (Fig. 5). Through Hoback Canyon, the T2 strath height is 10–13 m above the modern river. In the 2–3 km reach downstream of the Hoback normal fault, within the local basin, the strath vanishes beneath alluvium. It then reemerges downstream along the lower Hoback reach and the Snake River bedrock canyon between river km 0–2 at a height of 6–12 m. The T2 strath lowers to 4–6 m in the subsequent alluvial reach between river km 3.5–23 (Figs. 4–5). Toward the mouth of Alpine Canyon from km 23–39, the T2 strath height gradually increases and reaches up to 11 m (Figs. 4–5).

Tributary fan deposits are numerous along the canyon and typically interfinger with or prograde over mainstem terrace deposits. In places where tributary fan deposits prograde over T3 deposits at river km 17.5, 21.5, 27, and 33.5, the tributary fan deposits limit the thickness of the T3 deposits (Item S1). Terraces are in places beveled into old landslide deposits, for example at river km 3.5 and 17. Landslides are most common in areas underlain by the Lower Cretaceous Aspen and Bear River Formations (Item S1).

Terrace Chronology, Fault Offset, and Incision Rates

OSL ages for the T3 terrace deposits fall between 97 ka and 69 ka (Table 1 and Fig. 4). These thick T3 deposits have alluvial fills of >30 m that would have filled the entire valley. Based on these ages, aggradation of the T3 terrace began prior to ca. 97 ka and proceeded intermittently for up to 40 k.y. in this proglacial setting. We note that two samples within the Upper Snake River bedrock canyon appear to be stratigraphically reversed (USU-2080 and USU-2303, Fig. 4), although their ages are within one standard deviation. The samples are within meters of a strand of the Astoria fault, which was observed to offset T3 deposits (D. Rodgers and S. Wood, 2016, personal commun.). Late

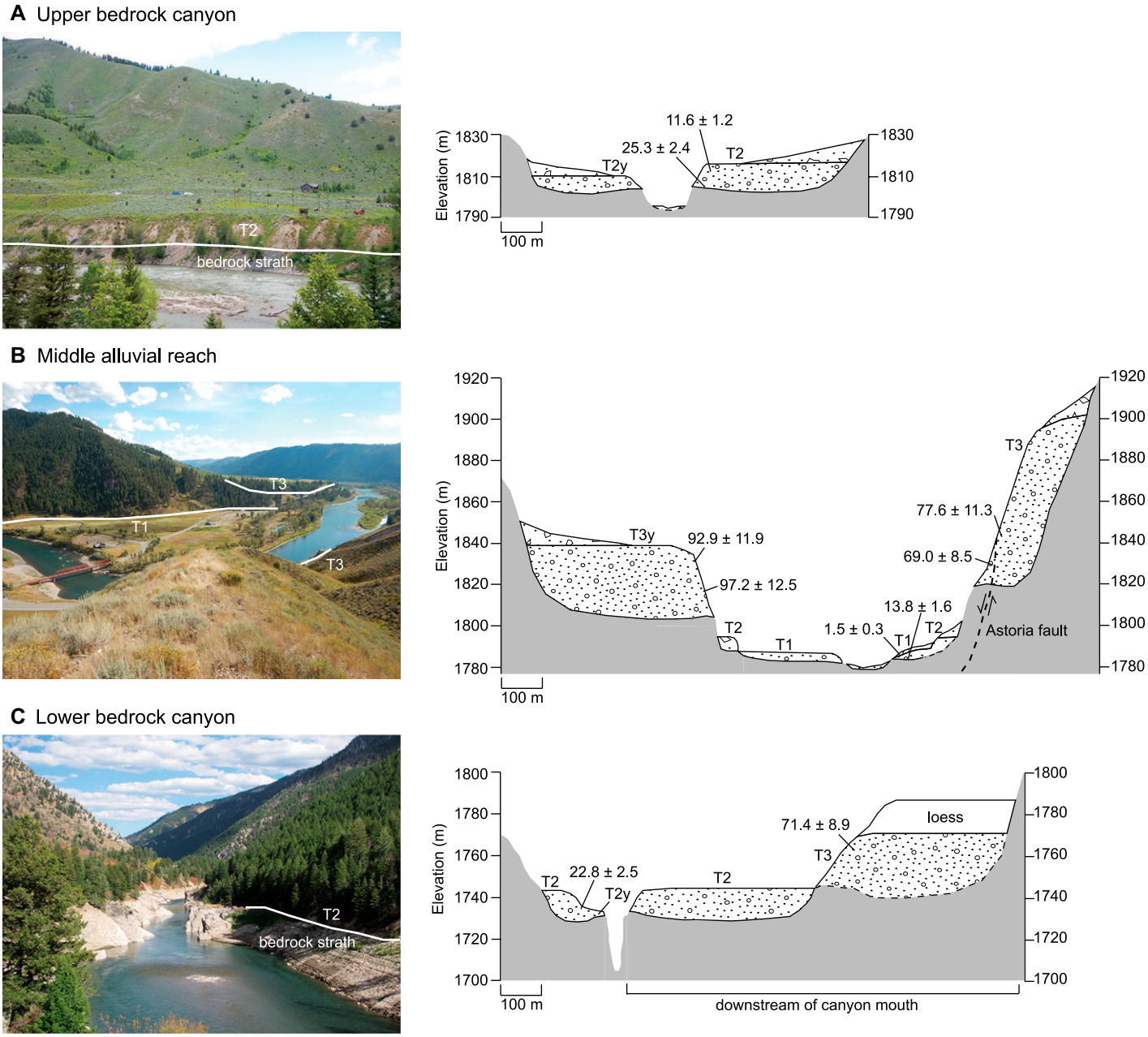

Figure 4. Composite cross sections and representative photographs include optically stimulated luminescence (OSL) ages for the upper bedrock canyon, middle alluvial reach, and lower bedrock canyon reaches. (A) Bedrock reach around Hoback Junction with dominant T2 strath terrace dated by OSL features a lower T2y fill-cut terrace. (B) Terrace deposits in the wide, braided alluvial reach near Astoria. Photo is pointed downstream from the top of the very thick T3 fill-terrace gravel, which is locally offset by the Astoria fault. (C) Cross section of T2 and T3 fill terraces at the mouth of the canyon near Alpine. The photo is aimed upstream into canyon during low level of the Palisades Reservoir, which typically drowns the mouth of the canyon. Note the narrow canyon and the high strath of the T2 terrace.

Quaternary offset could explain the age reversal as the lower OSL sample is broadly within the fault zone, and it may also cause the apparent ~15–20 m elevation difference in the T3 strath height between the river-right (north) bank at Astoria and the river-left (east) bank after the river turns south at this same point (Fig. 4B and see Fig. 2). If the T3 strath is indeed offset in this way by the fault, and taking the T3 strath age as ca. 100 ka, prior to major aggradation, late Quaternary slip rates on the Astoria fault may be on the order of 0.15–0.2 m/k.y. (150–200 m/m.y.). An alternative for the height difference in the strath may be the local preservation of higher valley-edge topography on the river-right (north) strath at Astoria.

Eight OSL samples collected from the T2 deposit constrain its age to between ca. 26 ka and 11 ka (Table 1). The T2 terrace along the Hoback River constrains Quaternary slip rates of the Hoback normal fault. Here, T2 ages vary between 14 ± 1.4 ka and 26 ± 2.4 ka in a sample taken at the mouth of Hoback Canyon in the near footwall of the fault. A clear scarp of this

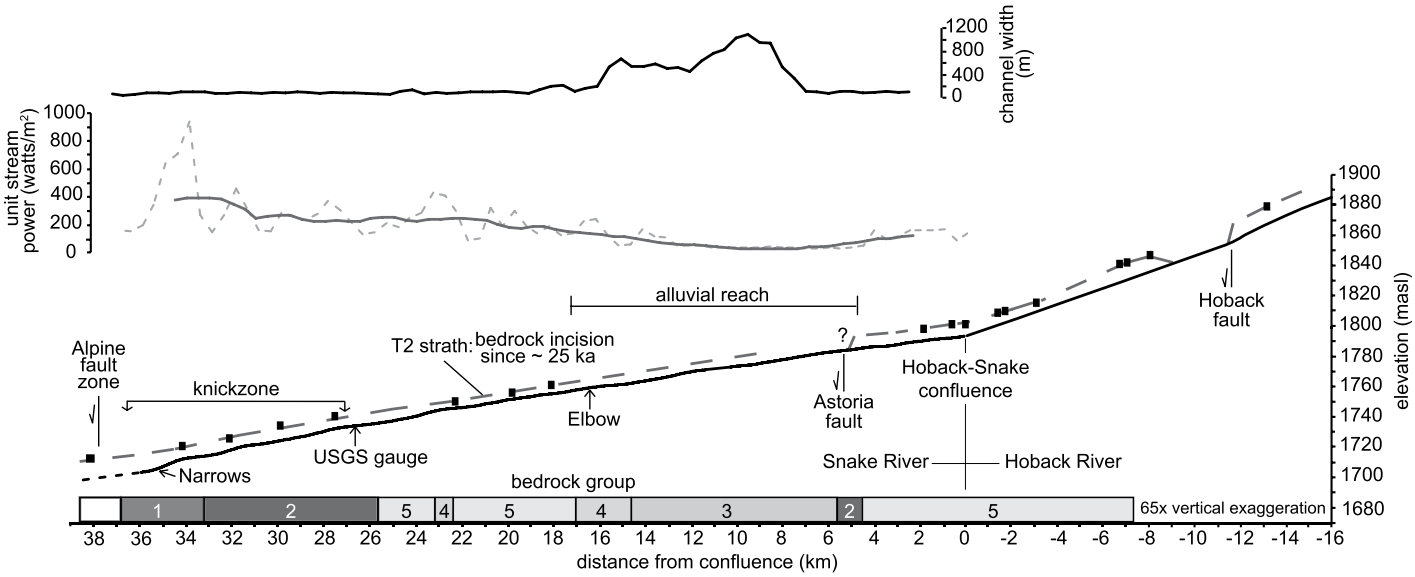

Figure 5. Longitudinal profile and topographic metrics along the profile of the lower Hoback and Snake Rivers through the studied reaches are shown. Upper graph marks channel width (black line) and stream power (gray lines) calculated along 500 m segments (dashed) and smoothed over a 5 km window (solid line). Lower graph marks the long profile of the Snake River; the water surface profile was recorded with a GPS from a raft and smoothed over a 500 m window (solid line). The long profile for the Hoback River was extracted from 1:24,000 scale U.S. Geological Survey topographic maps (USGS, 1965). Note the knickzone at the mouth of Alpine Canyon, where the river steepens and flows through limestones of bedrock groups 1 and 2. The dashed line is T2 bedrock strath height interpolated between surveyed points marked with black squares. Bedrock groups in the gray bar: Group 1—lower Paleozoic carbonates, Group 2—middle-upper Paleozoic carbonates, Group 3—lower Mesozoic sedimentary rocks, Group 4—middle Mesozoic sedimentary rocks, and Group 5—upper Mesozoic sedimentary rocks. Shade of gray represents percentage of resistant limestone from 100% (dark gray) to 0% (lightest gray).

fault, perpendicular to the river, offsets the T2 terrace tread by 3.5 m. If we assume abandonment of the tread at ca. 14 ka, the result is a slip rate of ~0.25 m/k.y. The T2 strath is offset by a minimum of 13 m across the trace of this structure, and with a minimum strath age of 26 ka, this suggests slip at up to 0.5 m/k.y. Thus, late Quaternary slip rates for the Hoback fault are broadly constrained to 0.25–0.5 m/k.y. (250–500 m/m.y.), which is potentially faster than the Astoria fault.

Finding datable sand in the low and thin T1 deposit proved challenging partly due to poor exposure. A single sample ostensibly collected from the base of a T1 strath, at river km 12 (USU-2302), returned an age of ca. 14 ka. We interpret this age as recording remnants of a T2 fill deposit below an erosional T1 terrace landform (Fig. 4B), and indeed the T1 is mapped as a beveled bedrock surface in the lower bedrock canyon. A single, late Holocene age (USU-2106) from a tributary deposit overlying the T1 in the alluvial reach suggests that the T1 is early to middle Holocene in age.

From our OSL chronostratigraphy, it is possible to estimate bedrock incision rates for the Upper Snake River over the past ~100 k.y. To integrate incision rates across climate-driven oscillations of aggradation and incision, we use the slope of trendlines in terrace-age-height space to illustrate incision through time (Fig. 6), and we plot the terrace chronostratigraphy from the upper alluvial reach and the downstream bedrock reach separately. Our record is less than ideal, because it includes only two deposits that vary in geometry and height across the study area and covers only 100 k.y. of time, and we note that the use of the modern channel as a datum leads to a maximum estimate of incision rates (Gallen et al., 2015). Estimated, longer-term incision rates cover a large range from ~150–600 m/m.y. (Fig. 6), and it is possible that incision rates may have increased over the 100 k.y. timeframe at the mouth of Alpine Canyon. Despite this broad overall estimate of the incision rate, the documented variation of the T2 strath height demonstrates that incision rates vary along the length of the Hoback and Upper Snake Rivers from potentially zero in the immediate hanging wall of the Hoback fault to maximum values in the footwall of the Hoback fault and in lower Alpine Canyon (Fig. 5).

Bedrock Strength

To help distinguish the effect of variable bedrock versus potential tectonic signals in drainage metrics, we investigate bedrock strength in the focus area through Alpine Canyon. Field-compressive strength measurements vary little in the folded and fractured limestones and sandstones of the study area (Item S3; see footnote 1). Selby rock mass strength (RMS) values, which combine average fracture spacing and weathering rankings with Schmidt hammer values (Selby, 1993), are also similar for all rock groups and classify all exposed strata as generally "strong" (Tuzlak, 2017). Selby rankings and Schmidt hammer values are limited because they ignore weakly consolidated shales. The proportion of shales is highly variable across the study area and clearly affects bulk rock-unit strength. When percentages of shale, sandstone/siltstone, and limestone in each bedrock group are tallied, older Paleozoic groups 1 and 2 are distinct in being composed of >57% of cliff-forming limestone with lesser amounts of shale and sandstone/siltstone (Item S3). In contrast, younger Mesozoic groups 3, 4, and 5 have <22% limestone and 44%, 71%, and 29% of shale, respectively (Item S3). These younger, shaley strata correspond to areas characterized by abundant landslides and gentler topography across the study area, yet the resistance of these bedrock groups does not necessarily explain channel metrics of the Snake River itself as discussed below.

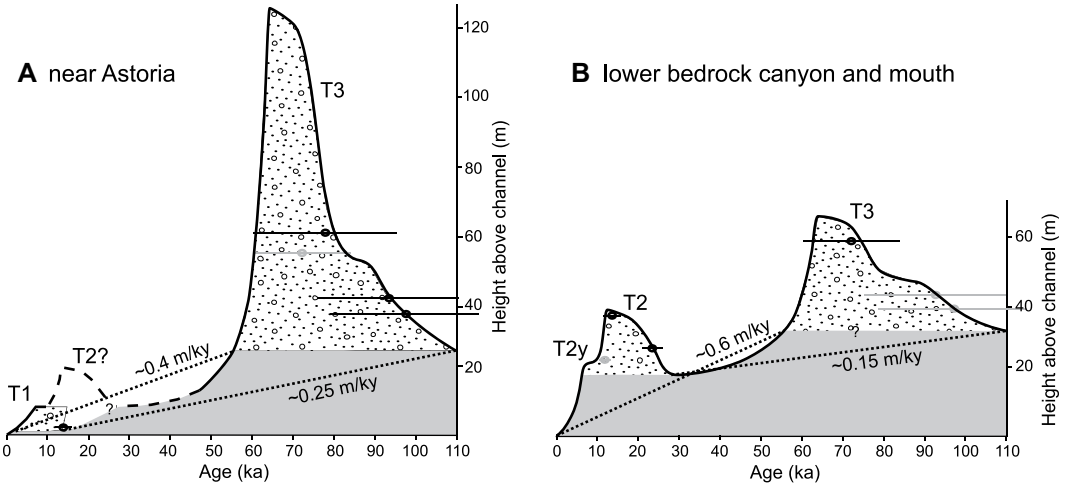

Figure 6. Incision rate estimates from terrace chronostratigraphy are provided for (A) alluvial reach near Astoria and (B) lower bedrock canyon and mouth. Optically stimulated luminescence ages with 1σ uncertainties are plotted if they are from samples within that reach and are in gray if they are from analogous deposits elsewhere in the study area. Thick black curve represents the elevation history of the river channel through time and over episodes of aggradation and incision. Straight dotted lines are background incision rate estimates integrating end-member strath positions over the high-amplitude aggradation incision cycles. Depending upon which positions are used, incision rates range from 0.15 m/k.y. to 0.6 m/k.y. (150–600 m/m.y.) across the study area and are highest at the mouth of Alpine Canyon; the general average is ~0.3 m/k.y. (~300 m/m.y.).

Mainstem Snake River Metrics

The Snake River is narrowest in the upper and lower bedrock canyons where the reach mean width is 77 m and 67 m, while the mean width of the intervening alluvial reach is 133 m, and the median width is much higher at 522 m (Figs. 5 and 7B). Similarly, the gradient of the river steepens, at river km 23 in Figure 5, as it cuts across the Snake River Range toward a knickzone at the mouth of the canyon. The overall increasing gradient in the lower bedrock canyon is observationally linked to the clustering of bedrock step-pool rapids in this section. In these downstream narrows of the bedrock canyon, the river channel is as narrow as 8 m between walls of resistant Paleozoic carbonates of bedrock groups 1 and 2 (Figs. 5 and 7). Given these gradient and width trends, unit stream power is highest in the upper and lower bedrock reaches, with an overall mean of 160 W/m^2 and 300 W/m^2, respectively, and a peak in the lower narrows of 1060 W/m^2 (Figs. 5 and 7C). In the alluvial reach, the mean unit stream power is only 115 W/m^2 and the median value is lower yet.

To assess whether these differences in Upper Snake River metrics correspond to changes in lithology, we compare gradient, width, and unit stream power within bedrock groups (Fig. 7). Note that bedrock group 3 only underlies the alluvial reach, where the direct influence of the underlying bedrock on the channel geometry is clearly limited. Gradient is generally lower in Mesozoic clastic rocks of groups 4 and 5 and higher in Paleozoic carbonates, especially those of group 1 (Fig. 7). Although landslides are abundant, specifically on hillslopes of shale-rich bedrock group 5, they do not seem to significantly increase river gradient (Fig. 7). This result is unsurprising given that the Snake River bed has exposed bedrock throughout the bedrock reaches where most group 5 rocks are encountered (Fig. 5) (Tuzlak, 2017). The Snake River is narrowest within bedrock group 1 (lower Paleozoic carbonates), where it has the highest mean unit stream power of 568 W/m^2 (Fig. 7). In contrast, channel sections through bedrock groups 2, 4, and 5 are wider and have mean stream power values that are less than half of those in bedrock group 1. The values associated with bedrock group 2 are notable. If bedrock strength alone controlled these measures, the reaches through carbonates of group 2 should match those underlain by the carbonates of bedrock group 1 instead of matching values of the shale-rich bedrock groups 4 and 5.

Tributary Steepness Analyses

Regionally, a contrast in channel steepness exists between the steep Gros Ventre, Wyoming, and Snake River Mountain Ranges and the gentler alluvial valleys (Fig. 8A). In more detail, within the Snake River Range, tributaries draining southwest or south into Alpine Canyon are distinctly steeper than those that drain the eastern slopes of the range (Figs. 8A and 9). Moreover, χ values show a strong contrast across the drainage divide of the Snake River Range north of Alpine Canyon (Fig. 8B; note that all drainages in this calculation were referenced to a common base level). For a subset of tributaries north of Alpine Canyon, we compare normalized channel steepness (k_{sn}) to the underlying bedrock type, which reveals overall higher (k_{sn}) values in older, more resistant Paleozoic carbonates compared to tributaries in Mesozoic sedimentary rocks (Fig. 7D). A t-test indicates that mean steepness index values of Paleozoic carbonate group 2 are higher than those of groups 3–5 to the 1% significance level. Similarly, the only channels on the east side of the Snake River Range that reach steepness values similar to those of the west side (e.g., Martin Creek) are underlain by those same carbonates. We note that the unexpectedly low median k_{sn} of group 1 carbonate rocks is difficult to interpret, because only four 500 m reaches in the region analyzed cross this bedrock type.

The longitudinal profiles of several tributaries (e.g., Fall, Martin, Bailey, and Indian Creeks) have distinct knickpoints, yet others in the study area do not (e.g., Cottonwood Creek) (Fig. 9). The χ profiles for tributaries illustrate well that these knickpoints, where they exist, have no systematic distribution (Fig. 10). The main tributary knickpoints occur at different elevations and coincide with geologic features or lithologic boundaries (for a full exploration, see Tuzlak, 2017). For example, the notable knickpoint along Bailey Creek, which enters Alpine Canyon at river km 17, is located on the downstream edge of a large landslide that dammed the creek and created a small lake (Fig. 9). Likewise, Indian Creek, which drains the Snake River Range into Palisades Reservoir, has a major knickpoint on the downstream edge of a landslide and debris flow deposit, and the mean k_{sn} in reaches upstream and downstream of the knickpoint is equivalent.

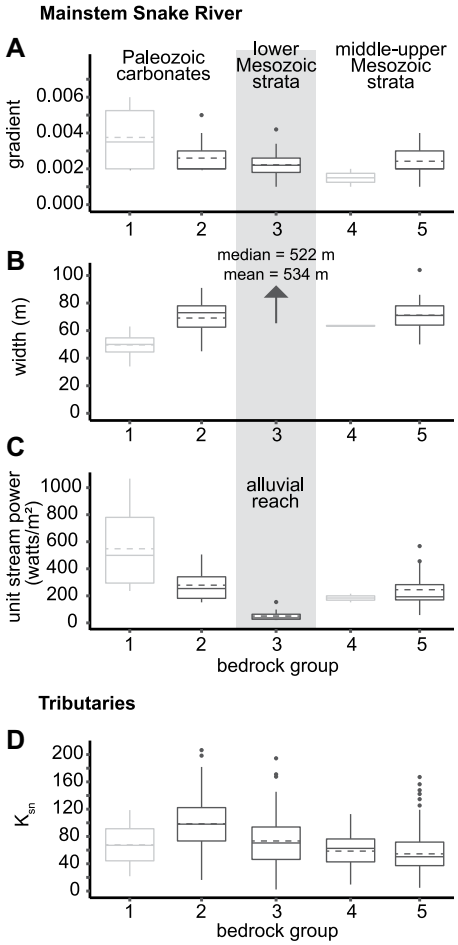

Figure 7. (A) Gradient, (B) width, and (C) unit stream power from 500 m reaches of the Snake River are organized by bedrock group. In cases where a 500 m reach is through two bedrock groups, the bedrock group with the greatest length was taken. Note the large variation of width and gradient in all reaches and no general trend of narrower width or steeper channels within more resistant bedrock groups 1 and 2. (D) Distribution of k_{sn} from Figure 8A is calculated along 500 m segments by bedrock group. For all box plots, the solid line is the median, the dashed line is the mean, boxes mark central quartiles, whiskers are 1σ variance, and dots are outliers. The k_{sn} values for group 2 are statistically different from those of group 3 to the 0.01 level of significance.

DISCUSSION

Incision Patterns and Rates from Terraces

The sequence of alluvial and bedrock reaches, and the terraces preserved along the lower Hoback River and the Snake River through Alpine Canyon, provide a broad and complex picture of Quaternary bedrock incision. Fluvial terrace deposits and landforms preserved along the study reaches, especially where they are associated with thick alluvial fills, represent significant temporal variation in aggradation and incision, which is associated with climate control that modulates overall bedrock incision in this proglacial setting. The preserved Quaternary record in the steep canyons of our study transect apparently lacks deposits from the Bull Lake (MIS 6) glaciation presumably due to subsequent erosion. Yet, the depositional ages of T3 deposits (ca. 110–60 ka) and T2 deposits (25–11 ka) correlate with colder episodes in regional climate records (Item S1). The period of aggradation of the T3 deposit from ca. 110–60 ka spans across MIS 5c to MIS 4 and includes two warmer and two colder intervals (Martinson et al., 1987). However, the best fit OSL ages cluster within two cold periods in this time period and correlate to a local record of loess deposition (Item S1) (Pierce et al., 2011). Possible sources for loess in this region are glaciogenic silts from nearby glaciations in Jackson Hole and the Yellowstone Plateau or from the eastern Snake River Plain (Pierce et al., 2011). Specifically, T3 deposit ages from three samples (USU-2019, 2080, and 2303) bracket the accumulation of a major loess sequence between 76 ka and 69 ka, and USU-1969 and USU-1998 fall within the previous regional loess dated to 99–91 ka (Pierce et al., 2011). Although no direct glacial deposits have been documented in regional records from this time (Licciardi and Pierce, 2018), this effusion of thick T3 gravel and the loess record imply some glaciation at times from MIS 5c to 4. The significant downstream thinning of the T3 alluvial fill from Astoria (~100 m) to the alluvial reach around the town of Alpine (~30 m) is also consistent with this hypothesis of a sediment source nearby at glacial termini in Jackson Hole and the Gros Ventre Range at that time, albeit the glacial extent was subsequently exceeded and overprinted by the Pinedale glaciation. Regardless, Pierce and Morgan (2009) hypothesized that only low and young (<25,000 ka) river terraces related to the last glacial maximum are present on the trailing margin of the hotspot track, but the T3 demonstrates that older terrace deposits are preserved.

All eight OSL ages from T2 gravels represent an episode of aggradation between ca. 25 ka and 11 ka. This range of ages coincides with MIS 2, a local pulse of loess deposition at 25–12 ka (Pierce et al., 2011), and the well-dated Pinedale glacial maximum in this region (Licciardi and Pierce, 2018). In general, episodes of aggradation coincide with colder periods identified in other regional climate records and support a link between terrace formation and glacial-interglacial cycles (e.g., Hancock and Anderson, 2002).

Our depositional ages directly constrain aggradation, when sedimentary and hydrologic conditions temporarily prevented bedrock incision due to channel-bed cover (e.g., Finnegan et al., 2007; Yanites and Tucker, 2010). Yet, the ages also indirectly constrain intervening episodes of incision and enable us to integrate over the late Quaternary to gain averaged incision rates that reflect rates of baselevel fall. Based on our data, bursts of incision occurred sometime between ca. 60 ka and 25 ka and then from 11 ka through today, generally during MIS 3 and MIS 1. Total incision rate estimates for the Snake River around Alpine Canyon only integrate over the past ~100 k.y. Nevertheless, they indicate background incision at roughly 300 m/m.y. and within a possible range of 150–600 m/m.y. over shorter parts of the late Pleistocene (Fig. 6). These rates are moderately rapid for the interior western U.S. (e.g., Dethier, 2001) and comparable to rates measured over similar timescales in the Upper Colorado River system (e.g., Darling et al., 2102; Pederson et al., 2013). This result of ~300 m/m.y. is also comparable to, or faster than, previous estimates on the leading, eastern edge of the Yellowstone hotspot along the Bighorn and Wind River systems (Reheis, 1985; Sharp et al., 2003; Pierce and Morgan, 2009; Guerrero, 2016).

Inquiry about more local spatial patterns of differential incision, especially as marked by the T2 strath, reveals that incision is fastest in the near-footwalls of the Grand Valley, Astoria, and Hoback faults (Fig. 5). In contrast, alluvial reaches with locally slower bedrock incision marked by the T2 strath coincide with the near-hanging walls of the same three normal faults, with incision logically reduced by subsidence of the hanging wall. In the cases of the Astoria and Hoback faults, we are able to provide the first rough constraints on late Quaternary slip. For the Astoria fault, a potential offset of the T3 strath suggests slip rates of ~0.15–0.2 m/k.y. (150–200 m/m.y.) over the past 100 k.y. Clearer constraints across the southern Hoback fault, with offset of the tread and strath of the T2, indicate somewhat faster slip rates between 0.25 m/k.y. and 0.5 m/k.y. (250–500 m/m.y.). These estimates are the first documentation of late Quaternary slip on these faults. It is notable that these faults have not been included in databases of active faults and seismic hazards, and we suggest that especially the southern Hoback fault should be included as such. Previous work on the greater Grand Valley fault system along the western mountain front of the Snake River Range and extending toward the Snake River

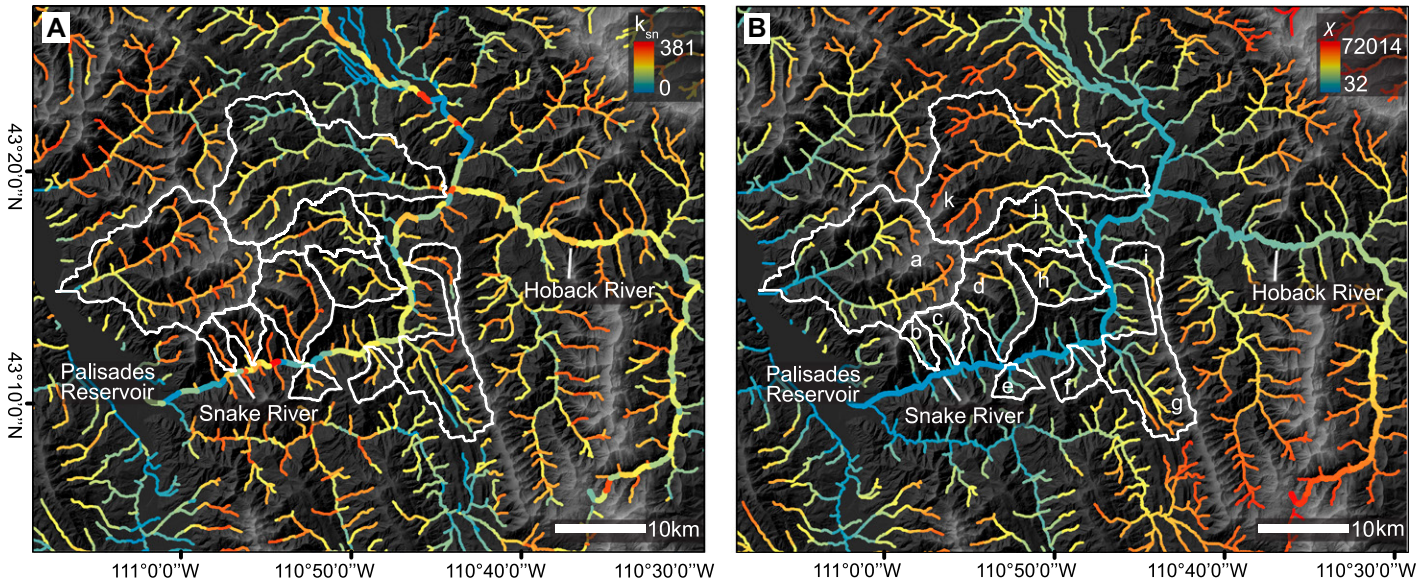

Figure 8. Map view plots are shown for (A) values of normalized steepness index (k_{sn}) and (B) χ for drainages in the study area with the common terrain model baselevel of Palisades Reservoir. Selected catchments are highlighted by white and are (a) Indian Creek, (b) Cottonwood Creek, (c) Red Creek, (d) Wolf Creek, (e) Roos Creek, (f) Pine Creek, (g) Bailey Creek, (h) Cabin Creek, (i) Martin Creek, (j) Dog Creek, and (k) Fall Creek. The k_{sn} values are from regressions along 1 km segments of tributaries with a reference concavity of 0.45. The χ values were calculated along 1 km segments using an A_0 of 1 km^2 and a best-fit m/n of 0.30. Note the higher k_{sn} values and lower χ values from tributaries draining the western slopes of the Snake River Range and lower k_{sn} values and higher χ on the eastern slopes.

Plain suggests that slip along the Grand Valley fault has declined through the Quaternary; there are no Holocene fault scarps present along most of its length north of Alpine (Piety et al., 1992). We have no direct measurements or observations of young offset along the Grand Valley fault, which lies just downstream of our study area. However, as we discuss below, the possibility that strands of this fault system have been active in the late Quaternary should be reconsidered.

Unraveling Tectonic and Lithologic Controls

The analysis of channel geometry and steepness may hold tectonic information if those channel characteristics can be distinguished from the effect of variable bedrock resistance. Along the Snake River, a prominent knickzone is apparent in the river gradient surveyed above the mouth of Alpine Canyon, and this reach is also characterized by a narrow channel and high stream power (Fig. 5). We argue that this knickzone cannot be fully explained by the relatively resistant Paleozoic carbonate rocks of bedrock group 1. The reach immediately upstream runs through measurably similar carbonates of bedrock group 2, yet the river gradient and unit stream power are significantly lower in that next upstream reach. In turn, channel metrics are all similar among rock groups 2, 4, and 5 across the focus area despite representing a range of lithologies from massive carbonates to more fractured sandstone and shales. Hence, the occurrence of the narrowest and steepest reach with the highest unit stream power does not seem to be a result of only lithology but also of other controls focused on the mouth of Alpine Canyon.

Differences in k_{sn} drainage steepness and χ values on the western side of the Snake River Range compared to the eastern side could be due to differential uplift and eastward tilting of the range along the Grand Valley fault system along its west side (Fig. 10). Indeed, the western front of the Snake River Range is characterized by steep relief and apparent triangular facets flanking the mouth of Alpine Canyon, features typically associated with active faults. However, the spatial correlation between high steepness indexes and resistant lower Paleozoic rocks prevents a simple tectonic interpretation of this steepness pattern. Indeed, knickpoints are not co-located at similar elevations in tributaries of the Snake River in Alpine Canyon as would be expected for a simple uplift signal affecting the drainage network. They are either located at boundaries between weaker and more resistant rock types, or they occur downstream of landslides and debris flows (Figs. 9 and 10). Although tributary knickpoints generally do not provide a clear record of Quaternary tectonic activity, a possible exception is the knickzone at the mouth of Fall Creek (Fig. 10). This profile convexity is potentially related to activity along the Astoria fault zone steepening the lower 2 km of Fall Creek and potentially generating landslides.

The strong difference in χ values across the drainage divide of the Snake River Range north of Alpine Canyon could relate to a difference in bedrock resistance on either side of the divide, but the bedrock contact does not follow this divide and the χ pattern very well (compare Figs. 2 and 8B). χ may better reflect a disequilibrium in channel profiles due to a contrast in baselevel fall (Willett et al., 2014). In such a case, steep drainage basins with low χ values will expand, and drainage divides will move toward gentler basins with higher χ values.

In summary, even though some of the contrast in k_{sn} steepness across the Snake River Range is attributed to lithological variations, the stream network geometry captured by χ as well as the major Snake River knickzone at the mouth of Alpine Canyon, support the interpretation of differential baselevel fall downstream. This baselevel fall west of the Snake River Range may originate either along the Grand Valley fault system itself or by subsidence farther afield in the Snake River Plain.

Sources of Baselevel Fall and Regional Tectonic Implications

The terrace record and long profile analysis across the study area allow us to revisit the hypotheses about the tectonic drivers of river

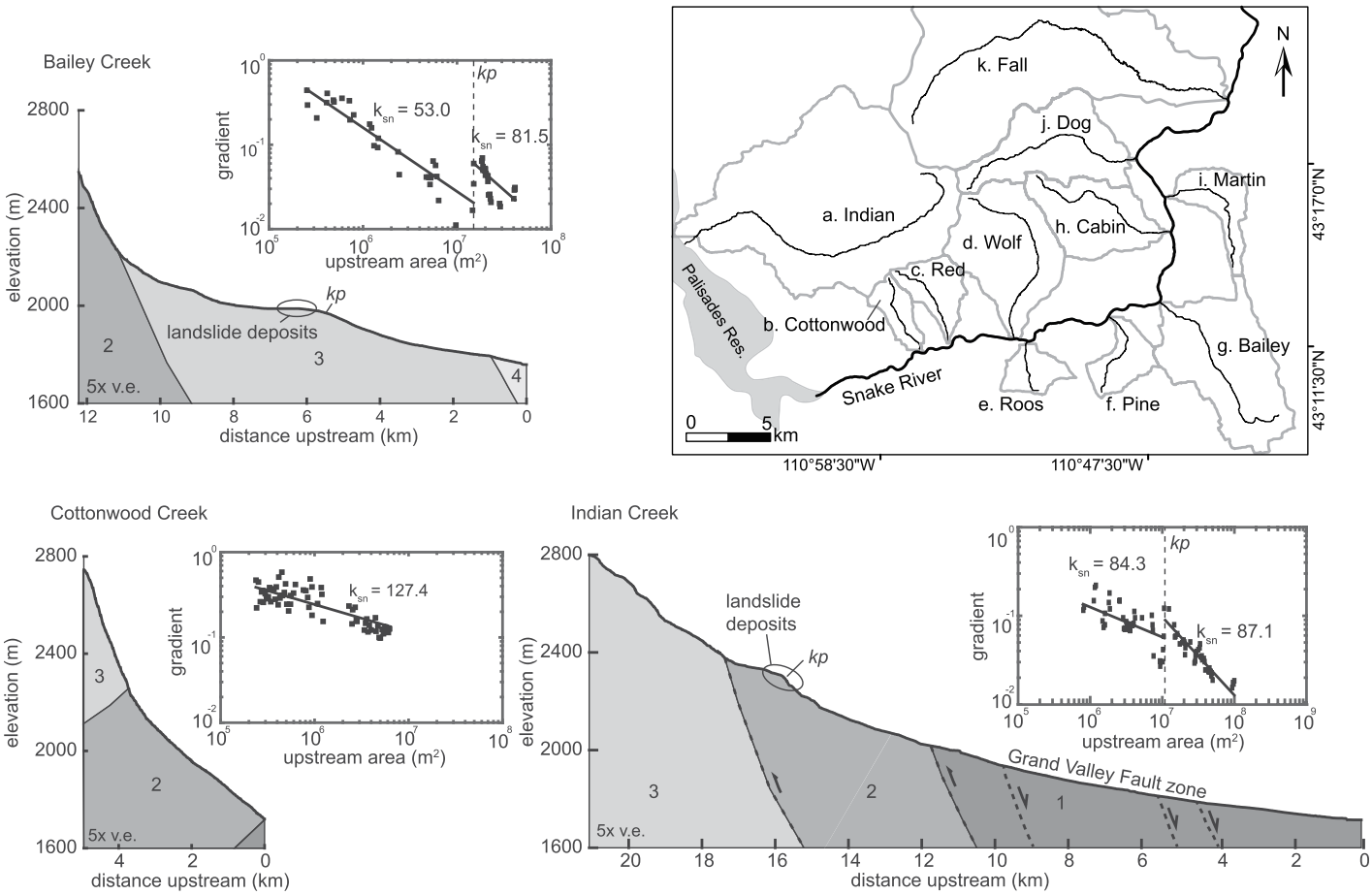

Figure 9. Longitudinal profiles and slope-area plots are given for example tributaries Bailey Creek, Cottonwood Creek, and Indian Creek that drain into the Snake River. Note that Indian Creek drains into Palisades Reservoir, and the lower profile and its confluence with the Snake River is not shown as it is obscured by the reservoir. Bedrock groups are labeled, and color denotes percentage of limestone from 100% (black) to 0% (white). Faults are represented as dashed lines, and bedrock contacts are solid lines. Slope-area plots show non-normalized reach concavity (θ) from a regression for reaches separated by knickpoints (*kp*) and normalized steepness index (k_{sn}) values. A reference concavity of 0.45 was used to calculate k_{sn}.

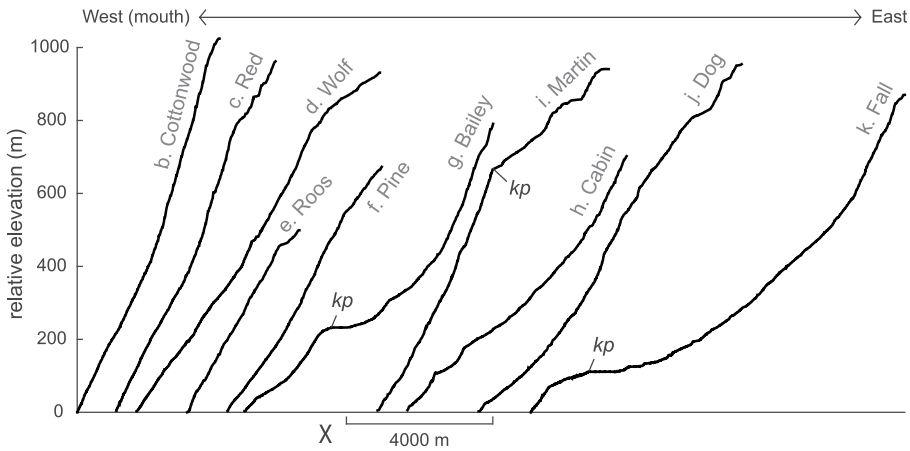

Figure 10. Chi plots of tributary profiles are arranged from west to east along the Snake River in the study area. A_0 = 1 km², and the best fitting m/n ratio for the trunk stream of tributaries is 0.30. Knickpoints (*kp*) are interpreted as having local, lithologic, or landslide controls. Note how tributaries draining into the western region of Alpine Canyon near the mouth are steeper than those further upstream.

incision laid out in Figure 3. Considering the long-wavelength potential deformation from either dynamic uplift along the Yellowstone crescent of high terrain or from subsidence downstream around the Snake River Plain, one of our first-order results is that terrace straths do not converge downstream in the pattern expected from the hypothesized uplift of headwaters (Fig. 3A). This finding contrasts with the downstream tilt of fluvial terraces on the leading margin of the Yellowstone hotspot along the Bighorn and Wind Rivers reported in previous work (e.g., Pierce and Morgan, 2009). Instead, terrace straths remain broadly parallel across our study transect except in lower Alpine Canyon, where straths rise above the channel and increasing incision and steepness culminates in the knickzone at the mouth of the canyon. Baselevel fall to the west, rather than uplift to the east, is supported by the pattern of χ steepness of the tributary stream network, which indicates a disequilib-

rium between steeper west-draining streams and gentler east-draining tributaries across the divide of the Snake River Range. Protracted, Neogene Snake River Plain subsidence to the west, downstream of our study area, may influence the incision of the Snake River Range. This downstream baselevel history is poorly known, and it is further complicated by the presence of early Pleistocene basaltic volcanism along the Snake River's path as it enters the Snake River Plain 50–90 km downstream of our study area (Moore and Embree, 2016). However, based on the apparent knickpoint at the mouth of Alpine Canyon, we suggest that Quaternary activity of the Grand Valley fault system, which marks the western mountain front of the Snake River Range, is a potential source of baselevel fall to the west. This fault system may be more complex and active than previously thought (Anders et al., 1989, Piety et al., 1992).

Our clearest finding matches the scenario of Figure 3C, where movement along individual normal faults is recorded by shorter-wavelength deformation of terrace straths. In the cases of the southern Hoback and Astoria normal faults, we are able to document them as active over the late Quaternary. Deformation along these faults, as recorded by the T2 strath, is localized in the immediate footwall and hanging wall areas. The Grand Valley fault system is more significant and forms the Snake River Range front and the basins that the Snake River follows downstream. Although direct evidence of late Quaternary slip has yet to be documented along the segments of this fault bounding the Snake River Range, we suggest the short-wavelength knickzone at the mouth of Alpine Canyon may be evidence of its activity. In overview, our results do not support a scenario of significant uplift along the hypothesized Yellowstone crescent of high terrain; instead, incision is segmented at shorter wavelengths by deformation along normal faults, which matches scenario C of Figure 3 and is also consistent with baselevel fall to the west toward the Snake River Plain. Future work exploring patterns of erosion more broadly at the leading and trailing edge of the Yellowstone system is warranted to understand the transient evolution of uplift and subsidence around the hotspot.

SUMMARY

Fluvial terrace deposits, channel long profiles, and topographic patterns provide clues to the Quaternary deformation patterns along a transect from the hypothesized Yellowstone crescent of high terrain toward the trailing margin of the Yellowstone hotspot, but these records are also complexly influenced by climate and variable bedrock. A rough, background incision rate estimate of ~300 m/m.y. over the past ~100 k.y. along the lower Hoback River and the Snake River through Alpine Canyon is moderate to high with respect to incision rates within the western U.S. and comparable to rates estimated on the leading margin of the Yellowstone hotspot. At shorter wavelengths, the patterns of incision from terrace straths and channel steepness reflect active slip on individual normal faults traversing the study area, which have not previously been documented as active and may have slip rates of 0.15–0.5 m/k.y. (150–500 m/m.y.). Varying bedrock resistance has a significant influence on the morphometry and steepness of smaller second to fourth order drainages in this study area, but broader patterns of χ and the major knickzone near the mouth of Alpine Canyon support a tectonic signal of baselevel fall to the west that is potentially associated with activity along the Grand Valley fault system or broader subsidence of the Snake River Plain. Furthermore, the pattern of terraces across the study transect is not consistent with broader wavelength uplift of the Yellowstone crescent of high terrain upstream. Generally, Quaternary incision and deformation on this transect across the southern margin of the hotspot are similar in overall rates but different in spatial pattern in comparison to what is interpreted from the leading eastern margin of the hotspot. Continued research to elucidate these patterns around the Yellowstone system is warranted.

ACKNOWLEDGMENTS

Field assistance was provided by Nick Smith, Nick Gottlieb, Sara Kelly, James Mauch, and Jackie Gottlieb, and assistance with optically stimulated luminescence data was provided by Michelle Nelson. Financial support was provided by Utah State University Geology Department, Geological Society of America, the Society for Sedimentary Geology, the Rocky Mountain Section Society for Sedimentary Geology, the Tobacco Root Geological Society, Utah State University Research and Graduate Studies, and the Salt Lake Chapter Association of Women in Geosciences. EarthScope AGeS Program geochronology student award funded by the National Science Foundation under Grant Nos. EAR-1358514, 1358554, 1358401, 1358443, and 1101100 (EarthScope National Office). We thank Andrew Meigs and an anonymous reviewer for detailed and constructive comments on an earlier version of the manuscript.

REFERENCES CITED

Anders, M.H., and Sleep, N.H., 1992, Magmatism and extension: The thermal and mechanical effects of the Yellowstone hotspot: Journal of Geophysical Research: Solid Earth, v. 97, p. 15,379–15,393, https://doi.org/10.1029/92JB01376.

Anders, M.H., Geissman, J.W.M., Peity, L.A., and Sullivan, J.T., 1989, Parabolic distribution of circumeastern Snake River Plain seismicity and latest Quaternary faulting: Migratory pattern and association with the Yellowstone hotspot: Journal of Geophysical Research: Solid Earth, v. 94, p. 1589–1621, https://doi.org/10.1029/JB094iB02p01589.

Anders, M.H., Rodgers, D.W., Hemming, S.R., Saltzmann, J., DiVenere, V.J., Hagstrum, J.T., Embree, G.F., and Walter, R.C., 2014, A fixed sublithospheric source for the late Neogene track of the Yellowstone hotspot: Implications of the Heise and Picabo volcanic fields: Journal of Geophysical Research: Solid Earth, v. 119, p. 2871–2906, https://doi.org/10.1002/2013JB010483.

Becker, T.W., Faccenna, C., Humphreys, E.D., Lowry, A.R., and Miller, M.S., 2014, Static and dynamic support of western United States topography: Earth and Planetary Science Letters, v. 402, p. 234–246, https://doi.org/10.1016/j.epsl.2013.10.012.

Beranek, L.P., Link, P.K., and Fanning, C.M., 2006, Miocene to Holocene landscape evolution of the western Snake River Plain region, Idaho: Using the SHRIMP detrital zircon provenance record to track eastward migration of the Yellowstone hotspot: Geological Society of America Bulletin, v. 118, p. 1027–1050, https://doi.org/10.1130/B25896.1.

Bridgland, D., and Westaway, R., 2008, Climatically controlled river terrace staircases: A worldwide Quaternary phenomenon: Geomorphology, v. 98, p. 285–315, https://doi.org/10.1016/j.geomorph.2006.12.032.

Burbank, D.W., Leland, J., Fielding, E., Anderson, R., Brozovic, N., Reid, M., and Duncan, C., 1996, Bedrock incision, rock uplift and threshold hillslopes in the northwestern Himalayas: Nature, v. 379, p. 505–510, https://doi.org/10.1038/379505a0.

Bursztyn, N., Pederson, J.L., Tressler, C., Mackley, R.D., and Mitchell, K.J., 2015, Rock strength along a fluvial transect of the Colorado Plateau—quantifying a fundamental control on geomorphology: Earth and Planetary Science Letters, v. 429, p. 90–100, https://doi.org/10.1016/j.epsl.2015.07.042.

Chang, W.-L., Smith, R.B., Wicks, C., Farrell, J.M., and Puskas, C.M., 2007, Accelerated uplift and magmatic intrusion of the Yellowstone caldera, 2004 to 2006: Science, v. 318, p. 952–956, https://doi.org/10.1126/science.1146842.

Chang, W.-L., Smith, R.B., Farrell, J., and Puskas, C.M., 2010, An extraordinary episode of Yellowstone caldera uplift, 2004–2010, from GPS and InSAR observations: Geophysical Research Letters, v. 37, no. L23302, https://doi.org/10.1029/2010GL045451.

Crosby, B.T., and Whipple, K.X., 2006, Knickpoint initiation and distribution within fluvial networks: 236 waterfalls in the Waipaoa River, North Island, New Zealand: Geomorphology, v. 82, p. 16–38, https://doi.org/10.1016/j.geomorph.2005.08.023.

Dethier, D.P., 2001, Pleistocene incision rates in the western United States calibrated using Lava Creek B tephra: Geology, v. 29, p. 783–786, https://doi.org/10.1130/0091-7613(2001)029<0783:PIRITW>2.0.CO;2.

Dorr, J.A., Jr., Spearing, D.R., and Steidtmann, J.R., 1977, Deformation and Deposition between a Foreland Uplift and an Impinging Thrust Belt, Hoback Basin, Wyoming: Geological Society of America Special Paper 177, 82 p.

Dorr, J.A., Jr., Spearing, D.R., Steidtmann, J.R., Wiltschko, D.V., and Craddock, J.P., 1987, Hoback River Canyon, central western Wyoming, *in* Beus, S.S., ed., Rocky Mountain Section of the Geological Society of America: Geological Society of America, Centennial Field Guide, v. 2, p. 197–200, https://doi.org/10.1130/0-8137-5402-X.197.

Duvall, A., Kirby, E., and Burbank, D., 2004, Tectonic and lithologic controls on bedrock channel profiles and processes in coastal California: Journal of Geophysical Research: Earth Surface, v. 109, no. F03002, https://doi.org/10.1029/2003JF000086.

Finnegan, N.J., Sklar, L.S., and Fuller, T.K., 2007, Interplay of sediment supply, river incision, and channel morphology revealed by the transient evolution of an experimental bedrock channel: Journal of Geophysical Research: Earth Surface, v. 112, no. F03S11, https://doi.org/10.1029/2006JF000569.

Flint, J.J., 1974, Stream gradient as a function of order, magnitude, and discharge: Water Resources Research, v. 10, p. 969–973, https://doi.org/10.1029/WR010i005p00969.

Fuchs, M., and Owen, L.A., 2008, Luminescence dating of glacial and associated sediments: Review, recommendations and future directions: Boreas, v. 37, p. 636–659, https://doi.org/10.1111/j.1502-3885.2008.00052.x.

Galbraith, R.F., and Roberts, R.G., 2012, Statistical aspects of equivalent dose and error calculation and display in OSL dating: An overview and some recommendations: Quaternary Geology, v. 11, p. 1–27, https://doi.org/10.1016/j.quageo.2012.04.020.

Gallen, S.F., Wegmann, K.W., and Bohnenstieh, D.R., 2013, Miocene rejuvenation of topographic relief in the southern Appalachians: GSA Today, v. 23, p. 4–10, https://doi.org/10.1130/GSATG163A.1.

Gallen, S.F., Pazzaglia, F.J., Wegmann, K.W., Pederson, J.L., and Gardner, T.W., 2015, The dynamic reference frame of rivers and apparent transience in incision rates: Geology, v. 43, p. 623–626, https://doi.org/10.1130/G36692.1.

Gibbard, P.L., and Lewin, J., 2009, River incision and terrace formation in the Late Cenozoic of Europe: Tectonophysics, v. 474, p. 41–55, https://doi.org/10.1016/j.tecto.2008.11.017.

Goldrick, G., and Bishop, P., 1995, Differentiating the roles of lithology and uplift in the steepening of bedrock river long profiles: An example from southeastern Australia: The Journal of Geology, v. 103, p. 227–231, https://doi.org/10.1086/629738.

Gran, K.B., Finnegan, N., Johnson, A.L., Belmont, P., Wittkop, C., and Rittenour, T., 2013, Landscape evolution, valley excavation, and terrace development following abrupt postglacial base-level fall: Geological Society of America Bulletin, v. 125, p. 1851–1864, https://doi.org/10.1130/B30772.1.

Guerrero, E.F., 2016, Quaternary landscape evolution and the surface expression of plume-lithosphere interactions in the Greater Yellowstone Area [Ph.D. thesis]: Corvallis, Oregon, USA, Oregon State University, 125 p.

Hancock, G.S., and Anderson, R.S., 2002, Numerical modeling of fluvial strath-terrace formation in response to oscillating climate: Geological Society of America Bulletin, v. 114, p. 1131–1142, https://doi.org/10.1130/0016-7606(2002)114<1131:NMOFST>2.0.CO;2.

Heller, P.L., Bowdler, S.S., Chambers, H.P., Coogan, J.C., Hagen, E.S., Shuster, M.W., Winslow, N.S., and Lawton, T.F., 1986, Time of initial thrusting in the Sevier orogenic belt, Idaho-Wyoming and Utah: Geology, v. 14, p. 388–391, https://doi.org/10.1130/0091-7613(1986)14<388:TOITIT>2.0.CO;2.

Howard, A.D., and Kerby, G., 1983, Channel changes in badlands: Geological Society of America Bulletin, v. 94, p. 739–752, https://doi.org/10.1130/0016-7606(1983)94<739:CCIB>2.0.CO;2.

Huang, H.-H., Lin, F.-C., Schmandt, B., Farrell, J., Smith, R.B., and Tsai, V.C., 2015, The Yellowstone magmatic system from the mantle plume to the upper crust: Science, v. 348, p. 773–776, https://doi.org/10.1126/science.aaa5648.

Huntley, D.J., Godfrey-Smith, D.I., and Thewalt, M.L., 1985, Optical dating of sediments: Nature, v. 313, p. 105–107, https://doi.org/10.1038/313105a0.

Jain, M., Murray, A.S., and Botter-Jensen, L., 2004, Optically stimulated luminescence dating: How significant is incomplete light exposure in fluvial environments?: Quaternaire, v. 15, p. 143–157, https://doi.org/10.3406/quate.2004.1762.

Kirby, E., and Ouimet, W., 2011, Tectonic geomorphology along the eastern margin of Tibet: Insights into the pattern and processes of active deformation adjacent to the Sichuan Basin, *in* Gloaguen, R., and Ratschbacher, L., eds., Growth and Collapse of the Tibetan Plateau: Geological Society, London, Special Publication 353, p. 165–188, https://doi.org/10.1144/SP353.9.

Kirby, E., and Whipple, K., 2001, Quantifying differential rock-uplift rates via stream profile analysis: Geology, v. 29, p. 415–418, https://doi.org/10.1130/0091-7613(2001)029<0415:QDRURV>2.0.CO;2.

Kirby, E., and Whipple, K.X., 2012, Expression of active tectonics in erosional landscapes: Journal of Structural Geology, v. 44, p. 54–75, https://doi.org/10.1016/j.jsg.2012.07.009.

Licciardi, J.M., and Pierce, K.L., 2018, History and dynamics of the Greater Yellowstone Glacial System during the last two glaciations: Quaternary Science Reviews, v. 200, p. 1–33, https://doi.org/10.1016/j.quascirev.2018.08.027.

Link, P.K., Fanning, C.M., and Beranek, L.P., 2005, Reliability and longitudinal change of detrital-zircon age spectra in the Snake River system, Idaho and Wyoming: An example of reproducing the bumpy barcode: Sedimentary Geology, v. 182, p. 101–142, https://doi.org/10.1016/j.sedgeo.2005.07.012.

Lowry, A.R., Ribe, N.M., and Smith, R.B., 2000, Dynamic elevation of the Cordillera, western United States: Journal of Geophysical Research: Solid Earth, v. 105, p. 23,371–23,390, https://doi.org/10.1029/2000JB900182.

Malatesta, L.C., Avouac, J.-P., Brown, N.D., Breitenbach, S.F.M., Pan, J., Chevalier, M.-L., Rhodes, E., Saint-Carlier, D., Zhang, W., Charreau, J., Lave, J., and Blard, P.-H., 2018, Lag and mixing during sediment transfer across the Tian Shan piedmont caused by climate-driven aggradation-incision cycles: Basin Research, v. 30, p. 613–635, https://doi.org/10.1111/bre.12267.

Martinson, D.G., Pisias, N.G., Hays, J.D., Imbrie, J., Moore, T.C., and Shackleton, N.J., 1987, Age dating and the orbital theory of the ice ages: Development of a high-resolution 0 to 300,000-year chronostratigraphy: Quaternary Research, v. 27, p. 1–29, https://doi.org/10.1016/0033-5894(87)90046-9.

McQuarrie, N., and Rodgers, D.W., 1998, Subsidence of a volcanic basin by flexure and lower crustal flow: The eastern Snake River Plain, Idaho: Tectonics, v. 17, p. 203–220, https://doi.org/10.1029/97TC03762.

Merritts, D.J., Vincent, K.R., and Wohl, E.E., 1994, Long river profiles, tectonism, and eustasy: A guide to interpreting fluvial terraces: Journal of Geophysical Research: Solid Earth, v. 99, p. 14,031–14,050, https://doi.org/10.1029/94JB00857.

Miller, J.R., 1991, The influence of bedrock geology on knickpoint development and channel-bed degradation along downcutting streams in south-central Indiana: The Journal of Geology, v. 99, p. 591–605, https://doi.org/10.1086/629519.

Montgomery, D.R., and Gran, K.B., 2001, Downstream variations in the width of bedrock channels: Water Resources Research, v. 37, p. 1841–1846, https://doi.org/10.1029/2000WR900393.

Moore, D.K., and Embree, G.F., 2016, Field guide to the recent volcanic history of the South Fork area between Swan Valley and Ririe, Idaho *in* Geology of the Eastern Snake River Plain and Surrounding Highlands: Tobacco Root Geological Society, 41st Annual Field Conference, Guidebook, p. 95–106.

Murray, A.S., and Wintle, A.G., 2000, Luminescence dating of quartz using an improved single-aliquot regenerative-dose protocol: Radiation Measurements, v. 32, p. 57–73, https://doi.org/10.1016/S1350-4487(99)00253-X.

Pazzaglia, F.J., Gardner, T.W., and Merritts, D.J., 1998, Bedrock fluvial incision and longitudinal profile development over geologic time scales determined by fluvial terraces, *in* Tinkler, K.J., and Wohl, E.E. eds., Rivers Over Rock: Fluvial Processes in Bedrock Channels: Washington, D.C., American Geophysical Union, p. 207–235, https://doi.org/10.1029/GM107p0207.

Pederson, J.L., Cragun, W.S., Hidy, A.J., Rittenour, T.M., and Gosse, J.C., 2013, Colorado River chronostratigraphy at Lee's Ferry, Arizona and the central Colorado Plateau bull's-eye of incision: Geology, v. 41, p. 427–430, https://doi.org/10.1130/G34051.1.

Perron, J.T., and Royden, L., 2013, An integral approach to bedrock river profile analysis: Earth Surface Processes and Landforms, v. 38, p. 570–576, https://doi.org/10.1002/esp.3302.

Peyton, S.L., Reiners, P.W., Carrapa, B., and DeCelles, P.G., 2012, Low-temperature thermochronology of the northern Rocky Mountains, western USA: American Journal of Science, v. 312, p. 145–212, https://doi.org/10.2475/02.2012.04.

Pierce, K.L., and Morgan, L.A., 2009, Is the track of the Yellowstone hotspot driven by a deep mantle plume? — Review of volcanism, faulting, and uplift in light of new data: Journal of Volcanology and Geothermal Research, v. 188, p. 1–25, https://doi.org/10.1016/j.jvolgeores.2009.07.009.

Pierce, K.L., Muhs, D.R., Fosberg, M.A., Mahan, S.A., Rosenbaum, J.G., Licciardi, J.M., and Pavich, M.J., 2011, A loess–paleosol record of climate and glacial history over the past two glacial–interglacial cycles (∼150 ka), southern Jackson Hole, Wyoming: Quaternary Research, v. 76, p. 119–141, https://doi.org/10.1016/j.yqres.2011.03.006.

Pierce, K.L., Licciardi, J.M., Good, J.M., and Jaworowksi, C., 2018, Pleistocene glaciation of the Jackson Hole area, Wyoming: U.S. Geological Survey Professional Paper 1835, 68 p, https://doi.org/10.3133/pp1835.

Piety, L.A., Sullivan, J.T., and Anders, M.H., 1992, Segmentation and paleoseismicity of the Grand Valley fault, southeastern Idaho and western Wyoming, *in* Link, P.K., Kuntz, M.A., and Piatt, A.B., eds., Regional Geology of Eastern Idaho and Western Wyoming: Boulder, Colorado, USA, Geological Society of America Memoir 179, p. 155–182, https://doi.org/10.1130/MEM179-p155.

Reheis, M.C., 1985, Evidence for Quaternary tectonism in the northern Bighorn Basin, Wyoming and Montana: Geology, v. 13, p. 364–367, https://doi.org/10.1130/0091-7613(1985)13<364:EFQTIT>2.0.CO;2.

Rhodes, E.J., 2011, Optically stimulated luminescence dating of sediments over the past 200,000 years: Annual Review of Earth and Planetary Sciences, v. 39, p. 461–488, https://doi.org/10.1146/annurev-earth-040610-133425.

Rittenour, T.M., 2008, Luminescence dating of fluvial deposits: Applications to geomorphic, palaeoseismic and archaeological research: Boreas, v. 37, p. 613–635, https://doi.org/10.1111/j.1502-3885.2008.00056.x.

Rodgers, D.W., Ore, H.T., Bobo, R.T., McQuarrie, N., and Zentner, N., 2002, Extension and subsidence of the eastern Snake River Plain, Idaho: Tectonic and magmatic evolution of the Snake River Plain Volcanic Province: Idaho Geological Survey Bulletin, v. 30, p. 121–155.

Schwanghart, W., and Scherler, D., 2014, TopoToolbox 2–MATLAB-based software for topographic analysis and modeling in Earth surface sciences: Earth Surface Dynamics, v. 2, p. 1–7, https://doi.org/10.5194/esurf-2-1-2014.

Selby, M.J., 1993, Hillslope Materials and Processes: Oxford, UK, Oxford University Press, 468 p.

Sharp, W.D., Ludwig, K.R., Chadwick, O.A., Amundson, R., and Glaser, L.L., 2003, Dating fluvial terraces by ^{230}Th/U on pedogenic carbonate, Wind River Basin, Wyoming: Quaternary Research, v. 59, p. 139–150, https://doi.org/10.1016/S0033-5894(03)00003-6.

Sklar, L.S., and Dietrich, W.E., 2001, Sediment and rock strength controls on river incision into bedrock: Geology, v. 29, p. 1087–1090, https://doi.org/10.1130/0091-7613(2001)029<1087:SARSCO>2.0.CO;2.

Smith, R.B., and Braile, L.W., 1994, The Yellowstone hotspot: Journal of Volcanology and Geothermal Research, v. 61, p. 121–187, https://doi.org/10.1016/0377-0273(94)90002-7.

Smith, R.B., Jordan, M., Steinberger, B., Puskas, C.M., Farrell, J., Waite, G.P., Husen, S., Chang, W.-L., and O'Connell, R., 2009, Geodynamics of the Yellowstone hotspot and mantle plume: Seismic and GPS imaging, kinematics, and mantle flow: Journal of Volcanology and Geothermal Research, v. 188, p. 26–56, https://doi.org/10.1016/j.jvolgeores.2009.08.020.

Stevens, A.L., Balgord, E.A., and Carrapa, B., 2016, Revised exhumation history of the Wind River Range, WY, and implications for Laramide tectonics: Tectonics, v. 35, p. 1121–1136, https://doi.org/10.1002/2016TC004126.

Stoeser, D.B., Green, G.N., Morath, L.C., Heran, W.D., Wilson, A.B., Moore, D.W., and Van Gosen, B.S., 2005, Preliminary integrated geologic map databases for the United States: Central States: Montana, Wyoming, Colorado, New Mexico, North Dakota, South Dakota, Nebraska, Kansas, Oklahoma, Texas, Iowa, Missouri, Arkansas, and Louisiana: U.S. Geological Survey Open-File Report 2005-1351, http://pubs.usgs.gov/of/2005/1351/.

Stoll, D., 1991, Neogene Basin filling history of the Grand Canyon of the Snake River, Teton and Lincoln Counties, Wyoming [M.S. thesis]: Idaho State University, Pocatello, Idaho, USA.

Tizzani, P., Battaglia, M., Castaldo, R., Pepe, A., Zeni, G., and Lanari, R., 2015, Magma and fluid migration at Yellowstone Caldera in the last three decades inferred from InSAR, leveling, and gravity mea-

surements: Journal of Geophysical Research: Solid Earth, v. 120, no. 2014JB011502, https://doi.org/10.1002/2014JB011502.

Tuzlak, D., 2017, Investigating patterns of fluvial form and incision near the Yellowstone Hotspot–Alpine Canyon of the Snake River, Wyoming [M.S. thesis]: Logan, Utah, USA, Utah State University, 115 p.

U.S. Geological Survey, 1965, Camp Davis and Bull Creek quadrangles, Wyoming: U.S. Geological Survey, scale 1:24,000, https://ngmdb.usgs.gov/topoview/viewer.

Vogl, J.J., Min, K., Carmenate, A., Foster, D.A., and Marsellos, A., 2014, Miocene regional hotspot-related uplift, exhumation, and extension north of the Snake River Plain: Evidence from apatite (U-Th)/He thermochronology: Lithosphere, v. 6, p. 108–123, https://doi.org/10.1130/L308.1.

Walker, E., 1964, Glacial terraces along the Snake River in eastern Idaho and in Wyoming: Northwest Science, v. 38, p. 33–42.

Wanless, H.R., Belknap, R.L., and Foster, H., 1955, Paleozoic and Mesozoic Rocks of Gros Ventre, Teton, Hoback, and Snake River Ranges, Wyoming: Boulder, Colorado, USA, Geological Society of America Memoir 63, https://doi.org/10.1130/MEM63-p1.

Wegmann, K.W., and Pazzaglia, F.J., 2009, Late Quaternary fluvial terraces of the Romagna and Marche Apennines, Italy: Climatic, lithologic, and tectonic controls on terrace genesis in an active orogen: Quaternary Science Reviews, v. 28, p. 137–165, https://doi.org/10.1016/j.quascirev.2008.10.006.

Wegmann, K.W., Zurek, B.D., Regalla, C.A., Bilardello, D., Wollenberg, J.L., Kopczynski, S.E., Ziemann, J.M., Haight, S.L., Apgar, J.D., Zhao, C., and Pazzaglia, F.J., 2007, Position of the Snake River watershed divide as an indicator of geodynamic processes in the greater Yellowstone region, western North American: Geosphere, v. 3, p. 272–281, https://doi.org/10.1130/GES00083.1.

Whipple, K.X., 2004, Bedrock rivers and the geomorphology of active orogens: Annual Review of Earth and Planetary Sciences, v. 32, p. 151–185, https://doi.org/10.1146/annurev.earth.32.101802.120356.

Whipple, K.X., DiBiase, R.A., and Crosby, B.T., 2013, Bedrock rivers: Treatise on Geomorphology, v. 9, p. 550–573, https://doi.org/10.1016/B978-0-12-374739-6.00254-2.

Willett, S.D., McCoy, S.W., Perron, J.T., Goren, L., and Chen, C.-Y., 2014, Dynamic reorganization of river basins: Science, v. 343, no. 1248765, https://doi.org/10.1126/science.1248765.

Wobus, C., Whipple, K.X., Kirby, E., Snyder, N., Johnson, J., Spyropolou, K., Crosby, B., and Sheehan, D., 2006, Tectonics from topography: Procedures, promise, and pitfalls, *in* Willett, S.D., Hovius, N., Brandon, M.T., and Fisher, D.M., Tectonics, Climate, and Landscape Evolution: Geological Society of America Special Paper 398, p. 55–74, https://doi.org/10.1130/2006.2398(04).

Yanites, B.J., and Tucker, G.E., 2010, Controls and limits on bedrock channel geometry: Journal of Geophysical Research: Earth Surface, v. 115, no. F04019, https://doi.org/10.1029/2009JF001601.

Science Editor: Brad S. Singer

Manuscript Received 25 September 2020
Revised Manuscript Received 22 March 2021
Manuscript Accepted 6 July 2021

Printed in the USA